The HL-LHC interaction region magnets towards series production

E. Todesco[1], H. Bajas[1], M. Bajko[1], A. Ballarino[1], S. Izquierdo Bermudez[1], B. Bordini[1], L. Bottura[1], G. de Rijk[1], A. Devred[1], P. Ferracin[1], P. Fessia[1], J. Fleiter[1], L. Fiscarelli[1], A. Foussat[1], G. Kirby[1], F. Mangiarotti[1], A. Musso[1], J. C. Perez[1], L. Rossi[1], S. Enomoto[2], T. Nakamoto[2], T. Ogitsu[2], M. Sugano[2], K. Suzuki[2], A. Bersani[3], B. Caiffi[3], P. Fabbricatore[3], S. Farinon[3], A. Pampaloni[3], S. Mariotto[4], M. Prioli[4], M. Sorbi[4], M. Statera[4], J. Garcia Matos[5], F. Toral[5], G. Ambrosio[6], G. Apollinari[6], M. Baldini[6], R. Carcagno[6], S. Feher[6], S. Stoynev[6], G. Chlachidze[6], V. Marinozzi[6], V. Lombardo[6], A. Nobrega[6], T. Strauss[6], M. Yu[6], M. Anarella[7], K. Amn[7], P. Joshi[7], J. Muratore[7], J. Schmalzle[7], P. Wanderer[7], D. Chen[8], S. Gourlay[8], H. Felice[8], I. Pong[8], S. Prestemon[8], G. L. Sabbi[8], L. Cooley[9]

[1] TE Department, CERN, Geneve, Switzerland
[2] KEK, Japan
[3] INFN, Sezione di Genova, Italy
[4] INFN, Sezione di Milano, Italy
[5] CIEMAT, Spain
[6] FNAL, USA
[7] BNL, USA
[8] LBNL, USA
[9] NHMFL, USA
E-mail: ezio.todesco@cern.ch

Abstract

The High Luminosity Large Hadron Collider (HL-LHC) is the new flagship project of CERN. Approved in 2013, it aims at a substantial upgrade of the collider to increase by a factor ten the statistics of the LHC data at the horizon of 2035-40. The upgrade relies on several cutting edge technologies; among them, large aperture superconducting magnets shall replace the present hardware to allow a smaller beam size in two interaction points. The project involves the construction of about 100 magnets of 6 different types: the quadrupole triplet, two main dipoles and three orbit correctors. The triplet, manufactured at CERN and in US, will consist of a series of 30 magnets relying of Nb_3Sn technology, with an operational peak field of 11.5 T. This will be the first miniseries of Nb_3Sn magnet to be installed in a particle accelerator. The other five magnets, all relying on Nb-Ti technology, and presenting non-trivial challenges in the design and construction, shall be manufactured under the responsibility of Japan, China, Spain, and Italy. The project is now in the phase of transition between the end of the prototype and beginning of the series construction. In this paper we review the magnet requirements and design, the technological challenges with respect to previous projects, and we summarize the steps that have been taken to validate the baseline.

1. Introduction

The Large Hadron Collider (LHC) is the particle collider with the highest energy ever built, colliding protons at 7+7 TeV energy [1]. The design of this accelerator relies on the 8 T Nb-Ti superconducting dipoles [2], pushing this technology to its limits for the large scale production of accelerator magnets [3]. First proposed in the 1980's [4], the LHC went through a design and prototyping phase in the 1990's [5,6,7], a construction and installation phase in 2000-2007 [3] and was finally commissioned in 2008-2010 [8]. It led to the discovery of the Higgs boson in 2012 [9,10], and to the award of a Nobel Prize in 2013.

One year before the Higgs boson discovery, the HL-LHC (High Luminosity LHC) design study was launched [11], aiming at a substantial upgrade of the LHC to increase the statistics of the collision data by a factor of ten. This design study was the last stage of a 10-years-long period of investigations on the possibility improving the LHC performances, started in 2000 [12,13,14].

The HL-LHC proposal [15,16] is based on a 20-fold potential increase of the collision rates (peak luminosity), given by a twice larger proton beam intensity (more fuel to burn) and a two times smaller beam size (fuel burnt more rapidly). Since the beam size in the Interaction Point (IP) is inverse proportional to the aperture of the first magnets after the experiments, a smaller beam size in the IP requires larger aperture magnets [12,13,14,15,16]. Therefore the HL-LHC project requires the replacement of the Interaction Region (IR) magnets with larger aperture magnets. The selected aperture of the IR magnets in HL-LHC is 150 mm [17], i.e. more than twice the 70-mm-aperture of the LHC IR magnets [18,19,20]. This larger aperture is used not only for reducing the beam size in the IP, but also for housing inside the magnet a 10-mm-thick tungsten beam screen [15,16]. This shield allows keeping the peak levels of the heat load and the radiation dose induced by collision debris as they in the LHC (5 mW/cm^3 and 35 MGy respectively).

An essential ingredient of the IR magnets upgrade is the triplet, that is the sequence of the first three quadrupoles in front of the experiments, needed to focus the particles back to the main dipoles and quadrupoles. To guarantee an adequate gradient in such a large aperture, a change of technology is required, i.e. going from Nb-Ti to Nb$_3$Sn, with peak field in the coils of the order of 11.5 T [17].

Large aperture Nb$_3$Sn quadrupoles were developed in the US since 2004 [21-26], firstly with 90-mm-aperture magnets (LARP-TQ) with two different mechanical structures, and successively with a 120-mm-aperture magnets (LARP-HQ) and with scaling of TQ short model to 3.7-m-long magnet (LARP-LQ). The final solutions adopted for HL-LHC [27,28,29] heavily rely on the R&D carried out in LARP, and

on the massive conductor development program [30] for Nb$_3$Sn launched by the US Department of Energy in 2000.

A special challenge of these magnets is the high level of stress in the coils induced by the electromagnetic forces, that is about twice what can be found in the 8 T LHC dipoles. In the HL-LHC triplet the stresses in the coil is not far from the 150 MPa; above this limit a degradation of the Nb$_3$Sn perfomance may occur [31,32]. Similar challenges are present for the 11 T magnet, a Nb$_3$Sn dipole magnet also planned for HL-LHC, in construction at CERN [33]. Both 11 T and MQXF magnets will provide precious information for the possible application of Nb$_3$Sn technology to future colliders [34-35], with magnets in the range of 12 to 16 T.

The IR magnets include not only the triplet, but also a separation and a recombination dipole, in the 4 to 6 T range, and three types of correctors in the 2 to 4 T range; for these magnets the Nb$_3$Sn technology is not needed, and they all rely on Nb-Ti. However, each of these magnets present interesting challenges to the superconduting technologies for accelerators. The 5.6 T separation dipole [36-43] has an unprecedented level of coil stress for Nb-Ti magnets due to the combination of very large aperture and large current density. The 4.5 T recombination dipole [44-46] has a special challenge in achieving a good field quality; the design is based on a similar concept developed for a D2 upgrade in [47], where an asymmetric coil compensates the magnetic coupling between the apertures. Asymmetric coils were succesfully manufactured for the combined function JPARC magnets [48].

The nested dipole corrector providing 2.1 T in both horizontal and vertical directions is based on a novel mechanical structure [49-51], with a double collaring and a mechanical lock between the horizontal and vertical dipole coils. The double aperture 2.6 T dipole corrector is based on a canted cosθ design [52-54], first proposed at the end of the 1970's [55], later industrialized in the US for several applications [56], and also proposed for high field magnets [57], but used for the first time in a CERN accelerator. The design is also quoted in the literature as titled solenoid or double helix. Finally, the high order correctors [58-64] rely on a superferric design (see for instance FAIR magnets [65] and SLHC prototypes [66], based on the same concept).

A very important feature of the accelerator magnets is the compactness. Contrary to experimental magnets in high energy physics, to MRI and NMR solenoids, and to magnetic systems needed for fusion, accelerator magnets must be extremely compact to fit the budget constraints of such large machines, requiring hundreds or thousands of these elements. Compact means using a very high current density of the order of 400 A/mm^2, i.e. 4 to 10 times larger than in the previously quoted devices. This introduces a series of challenges that are specific to these magnets [67], as the already mentioned large accumulation of stress, but also the

presence of training, instabilities, and a challenging protection system. For the HL-LHC triplet, a novel protection scheme, called Coupling Loss Induced Quench (CLIQ) has been developed at CERN and has been adopted as the baseline [68].

HL-LHC was endorsed as the flagship project of CERN in 2013 and eventually approved and financed in June 2016. Since then, the final phases of the conceptual and engineering design have been completed, and the prototyping phase is now coming to an end. The production shall last five years, and the magnets installation is foreseen for 2025-26. A special feature of this project is the relatively low number of magnets, that gives very little possibility of optimizing or fine tuning the design during production.

The six types of magnets are shared by six international collaborations, with CERN and a consortium of US laboratories (LBNL, FNAL and BNL) building the triplet, KEK building the separation dipole, INFN-Genova the recombination dipole, CIEMAT the nested correctors, IHEP the canted cosθ corrector and INFN-LASA the superferric correctors. CERN takes care of integrating the correctors in the cold masses of the main magnets.

The aim of this paper is to review the main design choices, both in terms of layout and in terms of magnet technology, and to describe in detail the validation of the design via the model and prototype manufacturing and via the power tests; the design of the cold masses and of the cryostat are not discussed in this paper.

The six different magnets are treated in separate sections, beginning with the magnets with a higher field, i.e. the triplet. Each section has a short description of the accelerator requirements and of the design choices, followed by the main body giving the design validation via power test. Additional paragraphs are dedicated to the design changes since the beginning of the project, to the open issues and setbacks, and to the project timeline. The six sections are preceded by a general one, dedicated to a review of the types of magnets, to the choices made for the layout, and to the main magnet design parameters.

2. Interaction region magnets layout and features

2.1 Lay-out and magnet requirements

The HL-LHC project requires 10 types of different magnets in the interaction regions around ATLAS and CMS:

- 3 types of main magnets: separation (MBXF) and recombination (MBRD) dipoles, and quadrupole triplets (MQXFA/B);
- 2 types of orbit correctors: single aperture nested correctors MCBXFA/B and double aperture correctors MCBRD;
- 1 skew quadrupole corrrector MQSXF;
- 4 types of nonlinear correctors: sextupole MCSXF, octupole MCOXF, decapole MCDXF and dodecapole MCTXF (installed in normal and skew configurations).

The lay-out of the LHC and of the HL-LHC are compared in Fig. 2.1.
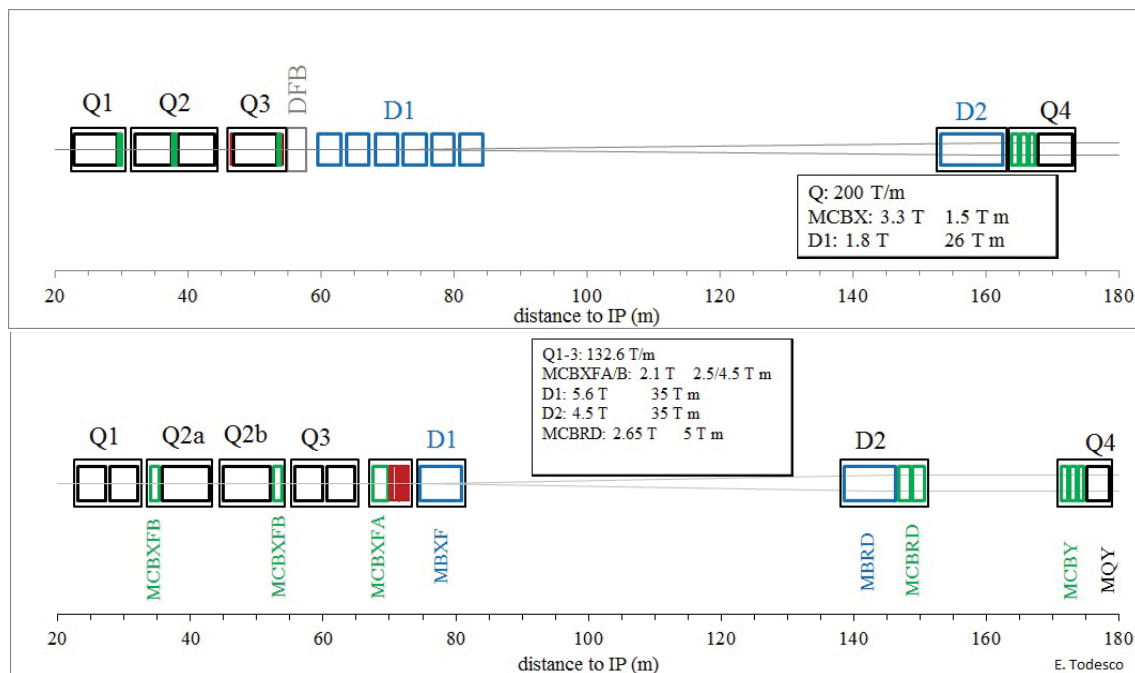
Fig. 2.1: The lay-out of the LHC interaction region (upper part) and of the HL-LHC interation region (lower part)

Thanks to the Nb₃Sn technology, the peak field is increased from 8 to 12 T, and therefore the triplet aperture is doubled, but the total length is increased by only 40% (25 to 35 m). The magnetic length is 8.4 m for Q1/Q3 and 7.15 for Q2a and Q2b [15,16,17]. The US collaboration, in charge of Q1/Q3, decided to split the magnet in two 4.2-m-long parts, to minimize the risks due to the length increase with respect to the 3.7-m-long magnet LQ, manufactured by LARP [25,26].

To make room for the additional 10 m of the triplet, and for the 20 m needed to install crab cavities between D2 and Q4, two steps are taken: (i) the 25-m-long resistive dipole D1 in LHC is replaced by a compact superconducting device (20 m saved). Moreover, (ii) the separation/recombination dipoles integrated field is increased from 27 to 35 T·m: this allows reducing the D1-D2 distance by another 20 m.

In HL-LHC the orbit correctors of the IR magnets are located (as in the LHC [1]) close to each quadurpole, but their strength is increased to 2.5 and 4.5 T·m. Additional orbit correctors of 5 T·m are located close to the D2 magnet; they are not present in the LHC layout. The nonlinear correctors, containing up to dodecapole components, are gathered in a special module between the triplet and D1. Skew dodecapole, and normal and skew decapoles are foreseen for HL-LHC and are not installed in the LHC.

The beam dynamics requirements on the magnetic lattice are realized with magnets characterized by a numerous set of parameters: among them, we will focus in the next section on what we consider as the most relevant in terms of superconducting technology.

2.2 Peak field and loadline fraction

The first main parameter we consider is the <u>peak field in the superconducting coil</u>. We use this quantity rather than the bore field since the HL-LHC magnets include not only dipoles, but also quadrupoles and higher order multipoles. We use the peak field rather than the maximum field at the magnet aperture (i.e., the gradient times the aperture radius for a quadrupole) since this is the quantity that sets the limits to the maximum current density in the superconductor, and therefore the requirement on the superconducting material. At 1.9 K, Nb-Ti can carry sizeable current densities to build accelerator magnets up to 8-10 T, and Nb₃Sn up to 14-16 T.

The second main parameter is the <u>loadline fraction</u>, defined as the ratio between the operational current and the maximum current tolerable to the superconductor in the magnet moving along the loadline (short sample current, see Fig. 2.2). This quantity is the condition in which the current density and the peak field in the coil reach the superconductor critical surface. The loadline fraction is therefore a number smaller than one, and the difference between one and the loadline fraction is defined in the

literature as loadine margin. In Fig. 2.2 we show the case of a Nb-Ti magnet, with 10 T short sample peak field and operational peak field at 7 T, with a 0.70 loadline fraction or a 30% margin on the loadline. The loadline fraction is one of the most discussed parameters in the design phase, since one has to find a compromise between large margin to guarantee a stable operation and a low rejection rate of the magnet production, and a small margin to limit the cost and the size of the magnets.
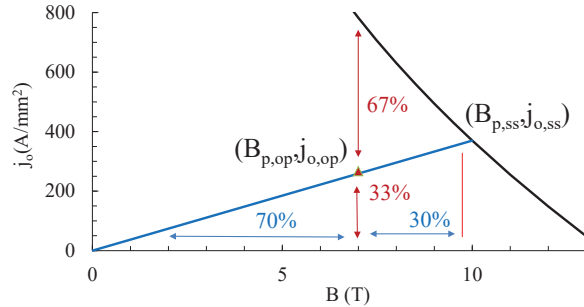
Fig. 2.2: Magnet loadline and critical surface; short sample condition (ss) and operational condition (op) are given.
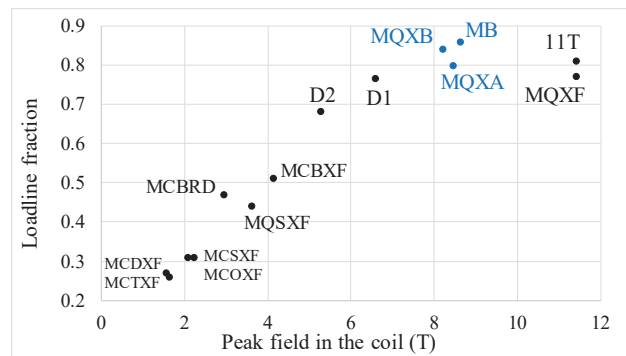
Fig. 2.3: Peak field in the coil versus loadline fraction of HL-LHC IR main magnets and correctors, 11 T, LHC main dipole (MB) and LHC IR quadrupoles (MQXA and MQXB).

In Fig. 2.3 we show for each type of HL-LHC IR magnet the position in the plot peak field in the coil vs loadline fraction. We can make the following considerations:

- For the most challenging magnet, i.e. the triplet, we have a 11.4 T peak field, requiring the use of Nb₃Sn, and a loadline fraction of 0.78. LARP quadrupoles had peak field of 10.4 T (TQ) and 11.0 T (HQ). [21,24]

- The project target is a loadline fraction just below 0.80, based on the LARP experience, that set both TQ and HQ at 0.80 [19-22]. Note that LHC dipoles were designed at a loadline fraction of 0.86 [1,3], operated at 0.43-0.50 (corresponding to 3.5-4 TeV

proton energy) in RunI, at 0.80 in RunII (corresponding to 6.5 TeV proton energy) [69,70], with the target of operating at 0.86 (7 TeV) in RunIII. The present triplet magnets [18,19] have loadline fraction between 0.80 and 0.84, and are now being operated at 6.5 TeV at 0.74 and 0.78 respectively.

For the other magnets there is a decreasing field and a decreasing loadline fraction (see Fig. 2.3), since the impact on cost and performance is lower, and one wishes to minimize the risk on these magnets.

- The separation dipole has a 6.5 T peak field, with a 77% loadline fraction. Initially it was set at 75%, and later was increased to reduce the magnet length to fit the KEK vertical test station.
- The recombination dipole has a 5.3 T peak field, with a more conservative 68% loadline fraction.
- Corrector magnets have a peak field ranging from 1.5 to 3.4 T, and are below 50% of the loadline fraction.

We also give the position of the 11 T dipole [29,33], that has few percent more loadline fraction with respect to the triplet, and the same peak field. All these values refer to nominal field, corresponding to 7 TeV operation. Following the LHC paradigm, the target of operation at 7.5 TeV (named ultimate current) should be possible for all hardware, without any engineering margin. All considerations in this section will be done for nominal current. In the next sections dealing with the test results, the level of nominal and ultimate current will be shown in all plots.

2.3 Current density and accumulated stress due to electromagnetic forces

In the absence of iron, the magnetic field created by a current flowing in a coil is proportional to the number of Ampere turns (number of turns of the coil times the current in the conductor). For superconducting magnets this equation is more adequate when written in terms of current density and coil width. For a typical sector coil of width w (see Fig. 2.4) the dipolar field is proportional to the current density times the coil width

$$B = \gamma j w \qquad (1)$$

with a constant γ that for a 60° sector is 6.9×10⁻⁷ T m/A [71]. Therefore the third main quantity we consider is the overall current density j, i.e. the Ampere turns divided by the area of the sector coil. For a quadrupole one has the logarithmic dependence

$$G = \gamma j \ln\left(1 + \frac{w}{r}\right) \qquad (2)$$

where r is the bore radius, and for a 30° sector the constant γ has the same value as for the dipole case [72]. For these

equations and constants, current densities are expressed in A/m². Note that in the following we will use the more practical units A/mm². With these current density units, the constants become 6.9×10⁻⁴ T mm/A for a dipole, with the width expressed in mm, and 0.69 T/m / (A/mm²) for a quadrupole, with a gradient expressed in T/m.
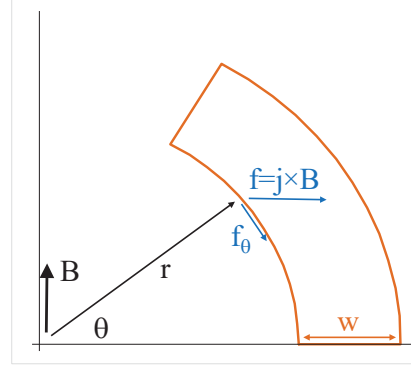
Fig. 2.4: Dipole sector coil of aperture radius r and coil width w (one quarter shown), and electromagnetic force on the coil edge assuming a field on the coil equal to the field in the centre.

Typical overall current densites in superconducting accelerator magnets range between 300 and 600 A/mm². Large current densites have the main advantage of giving a cheaper and more compact device. The price one has to pay for high current densities is related to three different aspects. First, the supercondutors for higher current densities tolerate lower fields. Second, high current densities increase the stress in the coil due to electromagnetic forces. Third, the magnet protection sets an upper limit of ~1000 A/mm² to the maximum current density. This is given by the balance between the energy density of the magnet over the winding and the heat capacity of the winding itself, that has to absorb the magnet energy during a quench without melting the coil. This limit is typical of main accelerator magnets (i.e. dipoles and quadrupole) where an energy extraction system for each magnet is not viable and/or affordable.

The fourth main parameter is the stress accumulation in the midplane. We recall that the force per unit of volume is given by the current density in the coil times the magnetic field in the coil. For a sector dipole, we carry out a first estimate of the midplane stress in the assumption that the field in the inner edge of the coil is equal to the field in the centre of the magnet (see Fig. 2.4). One can then integrate the azimuthal component fθ of the force over the inner bore, obtaining the midplane stress at the aperture radius r

$$\sigma_r = \int_0^{\pi/3} jBr \, \sin\theta \, d\theta = -\frac{1}{2} jBr \qquad (3)$$

where we considered a sector coil of 60º, canceling the sextupole component. For a quadrupole sector coil of 30º, in

with G denoting the quadrupole gradient. These simple estimates already gives a warning for the HL-LHC magnets: if the same parameters for field/gradient and current density were used, the 150 mm aperture gives a factor two increase with respect to the LHC IR magnets (70 mm aperture) and almost three with respect to the LHC main magnets (56 mm aperture).

The peak stress in the midplane inside the coil can be up to 50% larger than the stress at the bore radius r: this effect is particularly large for large coil widths, as discussed in the Appendix [73,74]. In Fig. 2.5 we show for the main HL-LHC IR magnets the position in the plot current density vs the maximum accumulated stress in the midplane, using the more refined estimate given in the Appendix. We also give the values for the 11 T, and for LHC main dipole (MB) and triplet magnets (MQXA and MQXB). Note that structure deformation is neglected in this analytical estimate. For the LHC MB and triplet magnets, one has two points since the coil is graded.
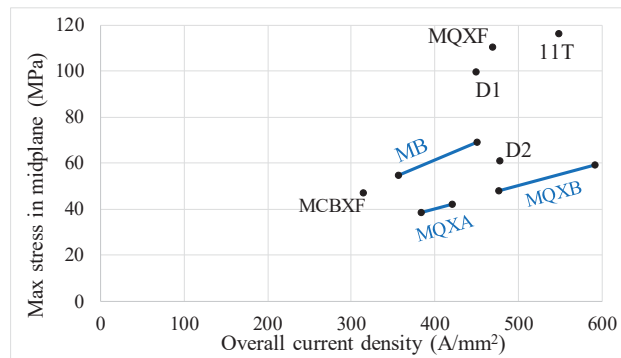
Fig. 2.5: Overall current density versus maximum midplane stress (in absence of structure and coil deformations) for HL-LHC IR main magnets, 11 T, LHC main dipole (MB) and LHC triplet (MQXA and MQXB).

We can make the following considerations:
- The HL-LHC triplet has a current density as in the outer layer of the LHC dipoles (used in the so-called low field region according to the grading technique). Compared to the inner layer of the LHC dipole, the triplet has 30% larger current density. Moreover, the accumulated stress in the midplane is about twice the LHC dipole. These aspects represent the main challenges (and advancements) with respect to the Nb-Ti technology.
- The separation/recombination dipoles have similar current densities to the triplet. The accumulated

the same hypothesis one gets

$$\sigma_r = -\frac{1}{4}jGr^2 \qquad (4)$$

stresses are much more critical for D1, whose level is around 100 MPa, close to the MQXF and to the 11 T. Therefore, even if the field is lower than the LHC dipoles, D1 is more challenging from the point of view of stress and current density. On the other hand, D2 and MCBXF do not show significantly larger challenges with respect to the LHC main dipole.
- The 11 T has a midplane stress close to the triplet: the much smaller aperture is compensated by the factor two between dipoles and quadrupoles, plus a 20% larger current density.

2.4 Energy density and protection

The fifth parameter we wish to comment on is the energy density in the coil. It is defined as the ratio between the magnet stored energy and the volume of the coil (insulated cable). This parameter is relevant to protection since in case of no energy extraction, the energy stored in the magnetic field has to be dissipated in the magnet coil, increasing its temperature. A intrinsic limit to the energy density is ~0.5 J/mm³, which correponds to the order of magnitude of the enthalpy needed to bring a typical insulated coil from 1.9 K to room temperature [75]. Obviously, the precise value depends on the fraction of insulation, of voids or of resin, and the ratio between the superconductor and the copper in the superconducting wire. The LHC dipoles and the LHC triplet have an energy density of ~0.05 J/mm³, and in the case of the HL-LHC we reach for the triplet ~0.10 J/mm³.

The sixth parameter is the copper fraction in the strand. In the triplet we have a copper non copper ratio of 1.2:1, i.e. 55% of the strand is composed by Cu. This ratio is much lower than in the LHC dipoles (62% and 66% in inner and outer layer respectively). This is done in increase the reduce the loadline fraction, i.e. to give more margin for the magnet operation. The price to pay is that with this coupling of energy density and copper fraction, one has about ~40 ms to detect the quench and induce a transition to a normal conducting state in the whole coil to stay below the 300 K hotspot temperature limit. In the LHC this time is ~100 ms for the outer layer, and ~200 ms for the inner layer, i.e. a factor 2.5 to 5 larger. This gives a quantitative idea of the unprecedented parameters that are being explored in the HL-LHC triplet in terms of protection. On the other hand, the other Nb-Ti magnets of HL-LHC do not pose particular challenges in terms of protection with respect to previous projects.

2.5 Summary table

We conclude this section by giving a complete list of the main magnet and dipole corrector parameters in Table 1. The detail of the design for each magnet shall be discussed in the next sections. The parameters of the skew quadrupole and of the high order correctors are given in Section 8.

Table I: summary of parameters of the main magnets of the HL-LHC interaction region and dipole correctors

		Triplet Q1/Q3 MQXFA	Triplet Q2a/b MQXFB	Short orbit corrector MCBXFB	Long orbit corrector MCBXFA	Separation dipole D1 MBXF	Recomb. dipole D2 MBRD	Orbit corrector MCBRD
Aperture[1]	(mm)	150	150	150	150	150	105	105
Field	(T)			2.10	2.10	5.60	4.50	2.60
Gradient	(T/m)	132.6	132.6					
Magnetic length[2]	(m)	4.20	7.15	1.200	2.200	6.26	7.78	1.92
Int field	(T m)			2.500	4.500	35.000	35.000	5.000
Int gradient	(T)	556.9	948.1					
Number of apertures		1	1	1	1	1	2	2
Distance between apertures[1]	(mm)						188	188
Number of circuits			4	8 / 8	4 / 4	4	4	16
Units needed		16	8	8	4	4	4	8
Spares		4	2	4	2	2	2	4
Cable data								
Material		Nb$_3$Sn		Nb-Ti		Nb-Ti	Nb-Ti	Nb-Ti
No. strands		40		18		36	36	
Strand diameter[3]	(mm)	0.850		0.480		0.825	0.825	0.825
Cu/NonCu		1.20		1.75		1.95	1.95	1.3
Cable thick. in.[3]	(mm)	1.530		0.819		1.362	1.362	
Cable thick. ou.[3]	(mm)	1.658		0.871		1.598	1.598	
Cable width[3]	(mm)	18.363		4.370		15.100	15.10	
Ins. thick radial[4]	(mm)	0.145		0.135		0.155	0.125	0.06
Ins. thick azimuth.[4]	(mm)	0.145		0.135		0.130	0.100	
Filling factor[5]		0.294		0.229		0.243	0.253	0.132
Coil design								
N. layers		2		2/2		1	1	2+2
N. turns/pole		50		140 / 191		44	31	3650
Cable length/pole	(m)	431	721	390 / 515	670 / 900	556	530	2200
Operational parameters								
Peak field[6]	(T)	11.4		4.13		6.58	5.26	2.94
Temperature	(K)	1.9		1.9		1.9	1.9	1.9
Current	(kA)	16.470		1.625 / 1.474	1.584 / 1.402	12.047	12.328	0.394
j overall[7]	(A/mm^2)	469		314 / 285	306 / 271	449	478	368
Loadline fraction[8]	(adim)	0.77		0.51	0.50	0.77	0.68	0.47
Temperature margin	(K)	5.0		4.1	4.1	2.4	3.0	4.2
Stored energy/m	(MJ/m)	1.17		0.064 / 0.119	0.061 / 0.109	0.340	0.291	0.074
Inductance/m	(mH/m)	8.21		48.7 / 105		3.97	3.52	480
Stored energy[9]	MJ	4.91	8.37	0.077 / 0.143	0.134 / 0.239	2.13	2.26	0.143

[1] aperture is the coil inner diameter at room temperature, excluding ground insulation, cold bore and beam screen;

[2] distance between apertures and magnetic length are given at 1.9 K;

[3] strand/cable dimensions are given at room temperature, after reaction for the Nb3Sn case;

[4] insulation dimensions are given at room temperature;

[5] filling factor is defined as the fraction of superconductor in the insulated cable;

[6] peak field in the coil is given including the contribution of the strand where the peak is located (usually called self-field correction);

[7] overall current density is average over the whole cross-section of the insulated cable (i.e. including voids or impregnation and insulation, but not copper wedges); for the MCBRD overall current density is referred to the cross-sectional area of the slot;

[8] loadline fraction is the ratio between the operational current and the short sample current on the load line;

[9] stored energy is given for the whole magnet: in case of independent apertures (MCBRD) or of nested magnets (MCBXF), stored energy is given for both circuits powered with maximum nominal current;

3. The triplet

3.1 Accelerator requirements

The triplet is a set of three quadrupoles, with equal and opposite gradients, alternating in the sequence +/-/+. Their optical function is to reduce the beam size in the cell arc by more than one order of magnitude. The integrated gradient is proportional to the beam rigidity (i.e. the beam energy divided by the charge of the particle). The integrated gradient is also inversely proportional to the focal length, i.e. to the distance of the triplet barycenter to the center of the experiment. Therefore, the gradient of the triplet ramps with the beam energy as the field of the main dipoles.

When the beam is injected, the optical functions in the interaction point are large (« unsqueezed »), i.e. the beam size is comparable to its value in the arcs. Morevoer, collisions in the interaction point are avoided through a small but sizeable (few millimeters) separation generated by the orbit correctors. After the beam reaches the maximum energy, the separation is removed, and the optical functions are squeezed in the interaction point. Note that the squeeze is done via the gradient of the matching quadrupoles (Q4 to Q7) : during this operation the triplet gradient is kept at its nominal value, corresponding to the beam rigidity and its focal length.

The triplet is usually made of four magnets, since the second unit is about twice as long as the first and the third, and therefore is usually split in two. In the HL-LHC, the four magnets are in a series on the same circuit with the proper order of the poles to guarantee the alternance of polarity. There is a trim on the first and last quadrupole to allow precise measurements of the optical functions around the experiments.

After the squeeze, the beam dynamics of the whole LHC is dominated by the triplet field errors. For this reason there are stringent requirements on the multipoles of the triplet at nominal energy. On the other hand, no requirements are given at injection energy. The triplet has about 1000 W of heat load, half of it being absorbed at higher temperatures (40-60 K) by a beam screen located inside the aperture. The most exposed parts (midplane of the coil) have an integrated dose of 35 MGy for the HL-LHC lifetime.

3.2 General design features

As stated in the introduction, the triplet magnets for the LHC upgrade were the object of a 20-year-long R&D program in the US ; it started [30] with a vigorous Nb_3Sn Conductor Development Program, and it was followed by the LHC Accelerator Research Program (LARP), aiming at the construction of several Nb_3Sn models of a 90-mm-aperture technological quadrupole TQ [21,22,23], and of three Nb_3Sn models of a 120-mm-aperture quadrupole HQ [24]. LARP

also succesfully demonstrated the first length scale-up of Nb_3Sn accelerator-type coils from 1 m to 3.4 m (LQ magnet [25,26]). All these programs were based on wind and react technique, a Rutherford cable insulated with a fiberglass sleeve, vacuum impregnation of the coil after heat treatment with CTD 101-K epoxy, and a two layer cos-theta layout for the coil. All these technical choices have been applied to MQXF. LARP explored two different mechanical structures, the first one based on stainless steel collars and a second one on Al shells, finding that the second one allows for assembly procedures with lower risk of damage to the brittle conductor. MQXF adopted the Al shell as mechanical structure. The last phase of LARP covered the design of MQXF in collaboration with CERN, the common program of short models, and the construction of two US-made long prototypes.

The MQXF coil is made up of two layers of the same conductor, arranged in 4 blocks (see Fig. 3.1), as in HQ. This lay-out guarantees enough free parameters to reach a accelerator-like field quality at nominal current. As in HQ, the alignment between the last cable of the inner block and the pole of the outer block is imposed, to have a layer jump that avoids any cable torsion. The only difference with respect to HQ is the scaling of the conductor width from 15 to 18 mm, to match the increased aperture. This is done by increasing the strand diameter from 0.8 mm to 0.85 mm, and increasing the number of strands from 35 to 40.
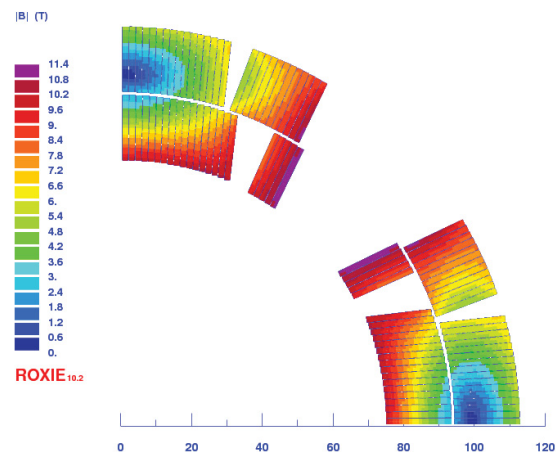
Fig. 3.1: MQXF cross-section, field map at nominal current.

3.3 Design features: strand and conductor

The conductor development program of US-DOE focussed on RRP Nb_3Sn wire produced by OST. The LARP strand workhorse was a 0.7 mm diameter wire (for TQ) and a 0.8 mm diameter wire (for HQ), based on the same 54/61 layout, reaching crititcal current values in the superconductor up to 3000 A/mm^2 at 12 T, 4.2 K. Note that 54/61 means that

there are 61 subelements, and 54 of them are Nb_3Sn, the other being Cu (see Fig. 3.2). This corresponds to filaments of a ~70 μm diameter. A 108/127 layout was also developed and used for HQ, having a filament diameter of ~50 μm. Layouts involving more filaments, as 132/169, were used in the MQXF short model program; eventually the 108/127 strand was adopted for the project, giving a good compromise between cost and filament size.
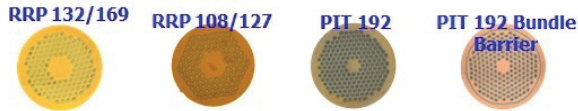
Fig. 3.2: Comparison of strand layout.

For MQXF, the minimal critical current requirement is 1280 A/mm^2 at 15 T and 4.22 K. RRR minimal requirement is 150 in the strand and 100 in the cable [76]. The cable degradation of critical current with respect to the unrolled strand has to be smaller than 5%.

CERN also supported an effort to develop a second provider based on a different technology [77], namely the PIT strand by Bruker, with 192 subelements (see Fig. 3.2). It has been used for the construction of two short models, the second one having a different strand layout including a bundle barrier.

3.4 Design features: coil manufacturing

Coil insulation and manufacturing follow the same technology adopted by the LARP program ; the insulation is a braided fiberglass. During winding, a ceramic binder is used to give rigidity to the coil ; the inner layer is cured to allow winding the second layer above it. The two layers are then reacted with three 50-h-long plateaux, the last one at 665º. This cycle was optmized to reach the best results in terms of j_c and RRR. The coil is then impregnated with CTD-101K, with a 5 hours at 110 C (curing) and 16 h at 125 C (post-curing).

3.5 Design features: structure

As said at the beginning of the section, the LARP structure developed for TQS and HQ, based on Al shell and bladder and key loading, has been selected [27] for MQXF as well (see Fig. 3.3). The coil pack is loaded in the Al shell at room temperature via bladders. The bladder pressure is an observable, so there is a very good control of the preload at room temperature. Once the desired value is obtained, keys are used to lock the structure and the bladders are removed. A stress of 40-60 MPa is imposed at room temperature.

During cool down, the Al shell shrinks more than the iron and the coil, and this increases the preload in the coil to 80-120 MPa. The iron structure (in blue in Fig. 3.3) has open

gaps according to the quadrupolar symmetry at room temperature and at 1.9 K. This means that during cool-down, all the pressure given by the shell thermal contraction ends up on the coil, with the exception of the pole alignment key. This key was inserted in HQ to guarantee the alignment of the coils. To be effective, it has to be in interference with the structure, and therefore it intercepts some stress coming from the Al shell, giving it an additional complexity. According to the short model program results, the pole key is probably unnecessary since magnetic measurements showed that coil alignment may be provided by a careful assembly of the coil pack also in absence of interference with the pole key.
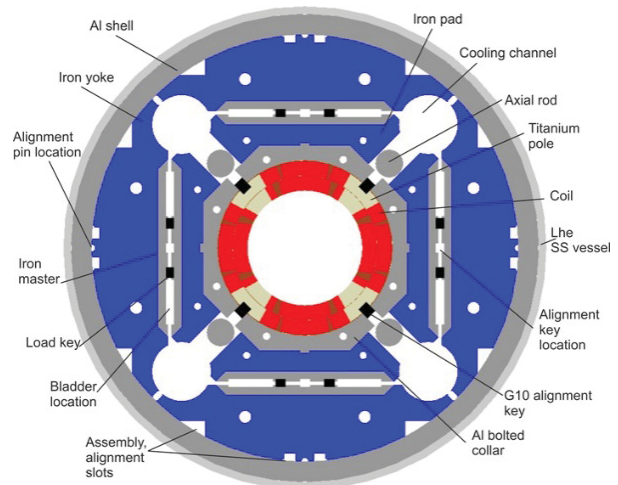
Fig. 3.3: Cross-section of the triplet quadrupole.

3.6 Design features: protection

The target maximum hotspot temperature of 350 K is reached via two complementary protection systems : outer layer quench heaters and CLIQ [78]. No energy extraction is present, as in all the main magnets of the HL-LHC interaction regions. The outer layer quench heater is made of a stainless steel strip, partially covered by Cu, deposited on a 50 μm polymide layer. The copper plating is done to focus the heat deposit in a series of 50-mm-long heating stations along the magnet length; this design is required for magnets longer than 1 m. This technology was initially developed for LHC, with 125-μm-thick polymide layer. In LARP, a 25 μm polymide layer was used; in HL-LHC the polymide thickness was doubled to 50 μm to increase the robustness of the insulation between the heaters and the coil. It had the negative side effect of increasing the quench delay from ~7 to ~15 ms, but still keeping the target of the 350 K maximum hotspot temperature in case of failures. Each half-coil has two strips (low field and high field), powered on 8 independent circuits for each quadrupole magnet.

CLIQ is a novel system, invented at CERN in 2010 [68], based on injecting a fast pulse of current in the coil to quench

the magnet via the heating induced by eddy currents. The pulse amplitude is 1.5 kA, and the period is ~70 ms (see Fig. 3.4). This double protection scheme guarantees a considerable redundancy. When both CLIQ and heaters are used, as it is in the baseline, the hotspot temperature is ~270 K. The same hotspot is found also in the case of protection via CLIQ only ; however, CLIQ does not protect the magnet below 3 kA. If CLIQ fails, quench heaters guarantee a ~310 K hotspot temperature. If quench heaters fail, CLIQ guarantees a ~270 K hotspot temperature. If CLIQ and one heater circuit fail, one has a 350 K hotspot temperature ; this is the assumed worse case scenario.
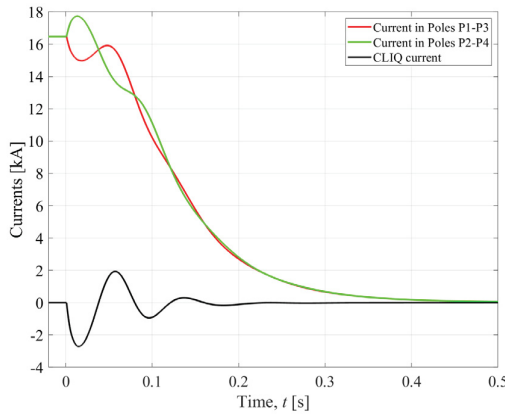
Fig. 3.4: CLIQ discharge.

3.7 Production data: strand

The strand production has been nearly completed for MQXFB [79]. The specification of j_c>1280 A/mm^2 at 15 T, 4.22 K corresponds to I_c>331 A, which is kept with a considerable margin (~10% larger on the lowest values, and ~15% larger in average, see Fig. 3.5). There has been a change in the heat treatment procedure to improve RRR, that was initially at the edge of the 150 specification and after billet 40 is well above 200 (see Fig. 3.6). The cable includes a stainless steel strip to control the dynamic effects; cabling is ongoing, showing no critical issues [80].

3.8 Production data: coil size

An essential ingredient of magnet manufacturing is reaching the nominal azimuthal dimension of the coils. A correct dimension of the coil allows reaching the prestress in the nominal position of the cable, i.e. achieving the required field quality and preload. A larger or smaller coil can be compensated via shim to achieve the target preload, but in this case the field quality is compromised. The second and even more important issue is the variation of the coil size along the magnet axis. If it becomes too large, this induces large variations of prestress that can degrade the cable or leave not enough prestress. The level at which the coil size

can be controlled should be of the order of ±0.1 mm, that is twice the tolerance of the impregnation mould. Over a MQXF coil, whose azimuthal length is 90 mm, this means a tolerance in relative of the order of ±0.1%, that with a Young modulus of the order of 15 GPa gives a precompression variation of ±15 MPa.
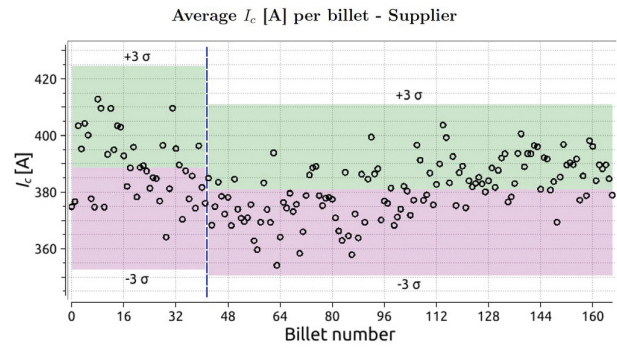
Fig. 3.5: Critical current along production of RRP strand.
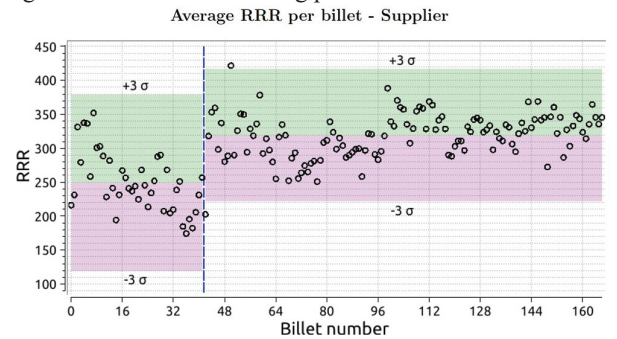
Fig. 3.6: RRR along production of RRP strand.

The short model coil production had a variation of average coil size within ±0.2 mm (see Fig. 3.7). For the US prototypes, the required ±0.1 mm was achieved (See Fig. 3.8); the CERN prototypes has not yet reached this level of spread along the magnet length. Moreover there is an offset of 0.2 mm due to an uncorrect sizing of the curing mold, that will be cured at the beginning of the series production.
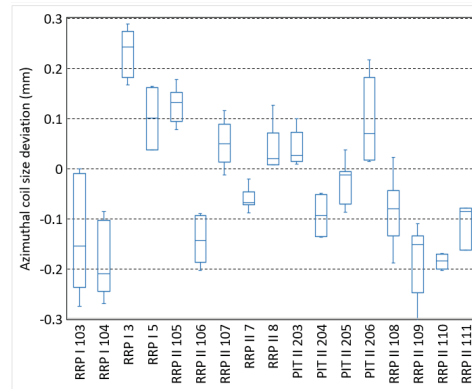
Fig. 3.7: Coil size for short models.
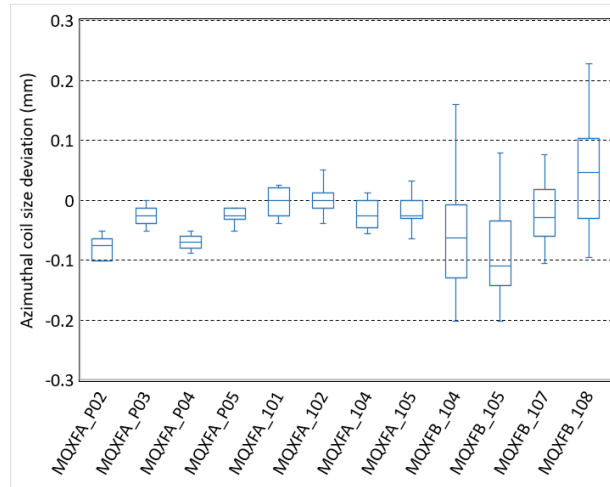
Fig. 3.8: Coil size for US (MQXFA) and CERN (MQXFB) prototypes.

3.9 Design validation via power tests: performance

The short model program is a joint venture between US LARP and CERN, with coils sharing the same design. Out of a total of 34 manufactured coils for short models, 21 coils were tested in 7 different assemblies, see Table II. Eight coils were made with the final RRP conductor (108/127) ; five coils were made with RRP with finer filaments (132/169) ; CERN manufactured coils with PIT 192 conductor, four of them with the initial layout and four with the bundle layout. Three structures were built at CERN, and one shipped to the US and used in the first short model MQXFS1. All coils reached nominal current with the exception of two PIT coils (208 and 209), that had non conform RRR.

As to the protoype program in the US, 13 coils were tested in four assemblies. The second prototype MQXFAP2 had a severe non conformity in one of the Al shells (see Section 3.11), and therefore coil data are not given here since they are not significant for this analysis. The other 9 coils reached nominal current. Two coils were completely manufactured by BNL, the others by FNAL, or wound by FNAL and completed by BNL.

Considering both short model and prototype, the histogram of quenches needed to reach nominal for each coil is given in Fig. 3.11, separating the different strands. Out of the 25 short coils reaching nominal current, 10 did it without quench, 9 with one quench and 2 with two quenches. We had four cases of 4 to 8 quenches needed to reach nominal, three from the early production using RRP 132/169 and one belonging to a mature production in FNAL with final strand. The detail of the test, including the different assembly conditions are given in the next section, the short model first and the US prototypes second, each category following the chronological order of the tests.

A short recall on the naming convention:

- Short models are identified by MQXFS;
- US prototypes are MQXFAP1 and MQXFAP2, the first one being 4 m long and the second with the final length (both manufactured by LARP);
- US-AUP series magnet are MQXFA03-23;
- CERN prototypes are MQXFBP1, MQXFBP2;
- CERN series is MQXFB01 to MQXFB10.

We now begin a detailed analysis of the performance history of each magnet.

Table II Summary table of manufactured coils and performance

Coil id.	Strand	Made in	Assembled in	RRR	I_c	Nominal reached	Quenches to nominal
3	RRP 108/127	FNAL/BNL	MQXFS1	244		Y	1
5	RRP 108/127	FNAL/BNL	MQXFS1	247		Y	2
103	RRP 132/169	CERN	MQXFS1	129	21.40	Y	4
104	RRP 132/169	CERN	MQXFS1	105	21.65	Y	1
7	RRP 108/127	FNAL	MQXFS3a	*178*		Y	1
8	RRP 108/127	FNAL/BNL	MQXFS3c	*182*		N (15.0-16.0)	
105	RRP 132/169	CERN	MQXFS3a	*155*	21.55	Y	5
			MQXFS3c			N (15.0-16.0)	
106	RRP 132/169	CERN	MQXFS3a	*160*	21.55	Y	0
			MQXFS3c			N (15.0-16.0)	
107	RRP 132/169	CERN	MQXFS3a	*135*	21.33	Y	1
203	PIT 192	CERN	MQXFS5	80	20.84	Y	0
			MQXFS6b			Y	0
204	PIT 192	CERN	MQXFS5	88	20.86	Y	2
			MQXFS6b			Y	0
205	PIT 192	CERN	MQXFS5	88	21.00	Y	1
206	PIT 192	CERN	MQXFS5	90	20.54	Y	1
108	RRP 108/127	CERN	MQXFS4	156	21.53	Y	0
109	RRP 108/127	CERN	MQXFS4	154	21.84	Y	0

110	RRP 108/127	CERN	MQXFS4	152	21.97	Y	1
111	RRP 108/127	CERN	MQXFS4	151	22.00	Y	0
208	PIT 192 w b	CERN	MQXFS6a	75	20.93	N (16.4)	(8)
209	PIT 192 w b	CERN	MQXFS6a	75	20.90	N (16.4)	(2)
210	PIT 192 w b	CERN	MQXFS6a MQXFS6b	90	20.51	N (16.4) Y	(0) 0
212	PIT 192 w b	CERN	MQXFS6a MQXFS6b	95	20.64	N (16.4) Y	(0) 0
P02	RRP 132/169	FNAL/BNL	MQXFAP1 MQXFAP1b	NA		Y	1
P03	RRP 144/169	FNAL	MQXFAP1 MQXFAP1b	NA		Y	7
P04	RRP 132/169	FNAL/BNL	MQXFAP1 MQXFAP1b	NA		Y	1
P05	RRP 108/127	FNAL	MQXFAP1	NA		Y	0
P06	RRP 108/127	FNAL	MQXFAP1b	NA		Y	2
110	RRP 108/127	FNAL	MQXFA03	214		Y	1
111	RRP 108/127	FNAL	MQXFA03	227		Y	8
202	RRP 108/127	BNL	MQXFA03	240		Y	0
204	RRP 108/127	BNL	MQXFA03	224		Y	0
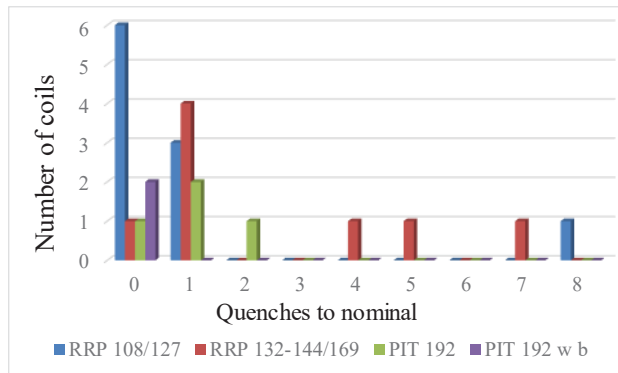
Fig. 3.9: Number of quenches to reach nominal current per coil.

The first short model MQXFS1 had two coils from CERN and two coils from LARP, made with RRP strand with different layouts (see Table II). The magnet was precompressed with ~100 MPa at 1.9 K, i.e. to prevent beginning of unloading up to 14 kA, i.e. 2 kA lower than nominal current, as confirmed by mechanical measurements (see Fig. 3.10, where the plateau in the stress-current curve is considered a sign of pole starting to unload). It reached nominal current (7 TeV operation, see 2.1) with 8 quenches (see Fig. 3.11), and ultimate current (7.5 TeV operation) with another 8 quenches. It reached the nominal current at 4.5 K and also after a thermal cycle without the need of additional training [81].

In a second assembly MQXFS1b, the precompression was increased to 120 MPa. This prevents unloading up to ~16 kA, i.e. close to nominal current, as confirmed by mechanical measurements (see Fig. 3.10). The magnet reached ultimate current without retraining, but showed some setbacks around ultimate (see Fig. 3.11, around quench n. 40-45).

A second iteration MQXFS1c on the magnet mechanics was done, increasing the axial precompression (see Fig. 3.12). The magnet reached nominal without quenches, and ultimate current with a slightly erratic behaviour in another 15 quenches. Finally, the magnet was used to test the assembly and welding of the stainless steel shell, included in the design as He containment, and showed similar behaviour to assemblies MQXFS1b and MQXFS1c. In total, the magnet underwent four thermal cycles and more than 100 quenches, always reaching nominal current without quench and, with some training and erratic behaviour, always reaching ultimate current [82]. This is the first short magnet to satisfy the performance requirements, showing a considerable operational margin and good properties in terms of memory (no retraining for nominal current).
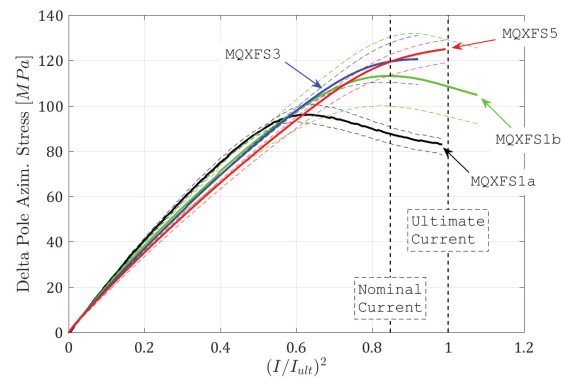
Fig. 3.10: Pole unloading in 3 short models: measured stress variation at the pole versus square of the current, normalized to ultimate current.
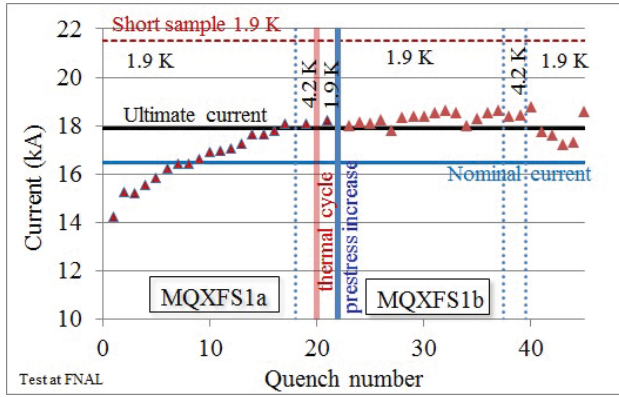
Fig. 3.11: Training of the short model MQXFS1 (first part).
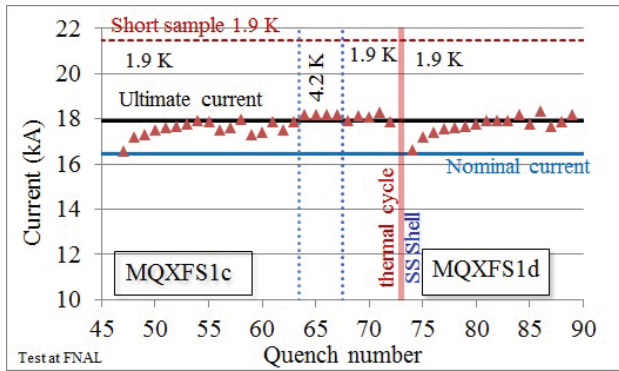
Fig. 3.12: Training of the short model MQXFS1 (second part).

The model MQXSF3, with three coils from CERN and one from LARP, was precompressed with 120 MPa, as MQXFS1b (see Fig. 3.10). The magnet reached nominal current with 8 quenches, but after reaching 17 kA it had a detraining in coil number 7 (see Fig. 3.13). The situation was unexpectedly recovered with a high ramp rate test, and 17 kA current was reached at 4.5 K. After a thermal cycle allowing to increase the axial prestress, the magnet was limited at 1.9 K just above nominal current (see Fig. 3.13, MQXFS3b), but reached 1.5 kA more at 4.5 K [83,84].
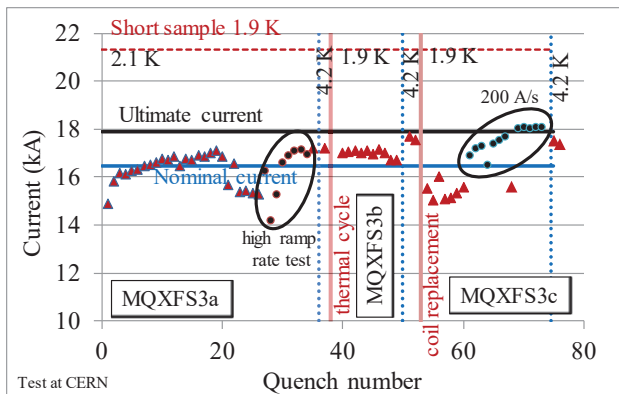
Fig. 3.13: Training of the short model MQXFS3

The limiting coil was replaced in assembly MQXFS3c, but another coil (number 105) was then blocking the magnet at 1.9 K well below nominal. This was a typical example of reverse behaviour, with the magnet better behaving at higher temperatures and higher ramp rates. Ultimate current was reached at 200 A/s ramp rate, and more than 17 kA at 4.5 K. This suggests the existance of a complex mechanism of performance limitation due to conductor instabilities. At the moment of writing we have no justification of the limited performance of this short model.

The short model MQXFS5 was manufactured with a PIT conductor at CERN. It was precompressed with 140 MPa., i.e. full precompression for ultimate current. Strain measurements confirmed the expected mechanical behaviour, i.e. no unloading at ultimate current (see Fig. 3.10). It reached nominal current with four quenches [83], and ultimate current with 26 additional quenches (see Fig. 3.14). Training was long but without any detraining. The magnet showed perfect memory at ultimate current, and a quench level at 4.5 K more than 1 kA above nominal. This is the second short magnet to satisfy the performance requirements, showing a considerable operational margin and extremly good properties in terms of memory (no retraining to ultimate current).
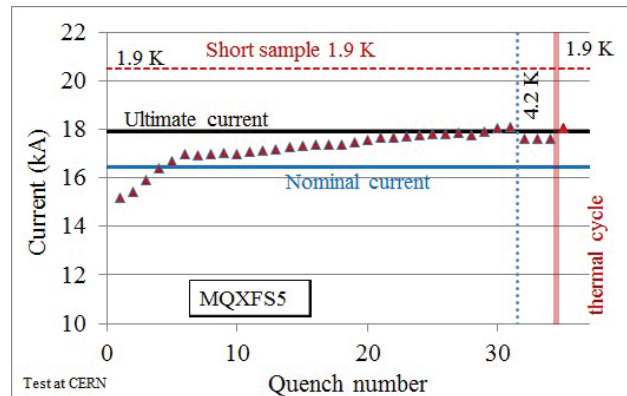
Fig. 3.14: Training of the quadrupole short model MQXFS5.

The short model MQXFS4 was the first one with four coils made with 108/127 RRP strand, corresponding to the solution adopted for the series magnets both in the US and at CERN. The coils were all manufactured at CERN laboratory 927. It was precompressioned with 120 MPa, an intermediate level that has been adpoted for all future magnets of the project. It reached nominal current with one quench (see Fig. 3.15), and ultimate current with four additional quenches [84]. The magnet had perfect memory at ultimate current, and reached ultimate current also at 4.5 K. It went through an endurance test, with 8 thermal cycles, showing no signs of degradation [82]. This is the third short magnet to satisfy the performance requirements.
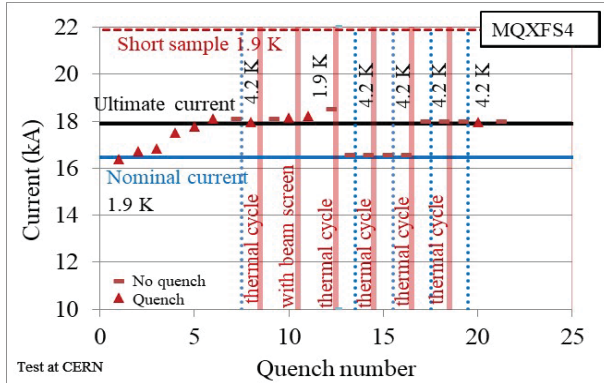
Fig. 3.15: Training of the quadrupole short model MQXFS4

The second layout for PIT strand (with bundle) was used to manufacture four coils that were assembled in MQXFS6. Two coils had extremely low RRR values, well below the specified values (75 vs a minimum allowed of 100). One of them was shown to be the limiting coil in the magnet, that barely reached nominal current (see Fig. 3.16). In this case there was no indication of reverse behaviour, as the magnet had worse performance with higher ramp rates and higher temperatures. The missing performance of MQXFS6 was attributed to the very low RRR coils, that were replaced with two coils of MQXFS5. The new assembly MQXFS6b reached utimate without quench, and was trained up to a record of 19.14 kA, corresponding to 93% of the short sample. After the thermal cycle, the magnet quenched above 19 kA, i.e. above 90% of the short sample, showing a spectacular potential of this technology. It also reached 98% of the short sample at 4.5 K. This is the fourth short magnet to satisfy the performance requirements.
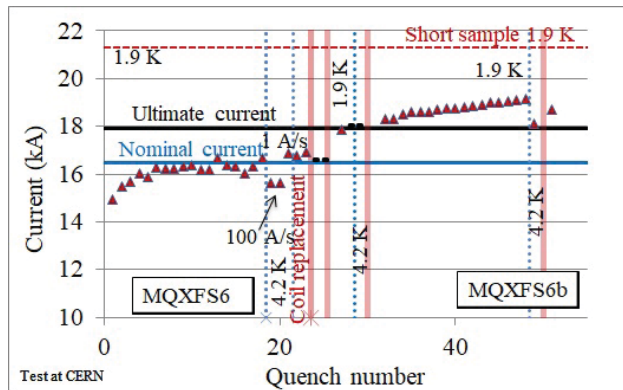
Fig. 3.16: Training of the quadrupole short model MQXFS6.

The first prototype from the US-LARP had 4-m-long coils, and RRP strand with different layouts (see Table II). The magnet trained to nominal current with 10 quenches (see Fig. 3.17), and test was stopped due an electrical short, with the current 1 kA above nominal current after 17 quenches.

This magnet proved the ability to reach nominal on a 4-m-long model.
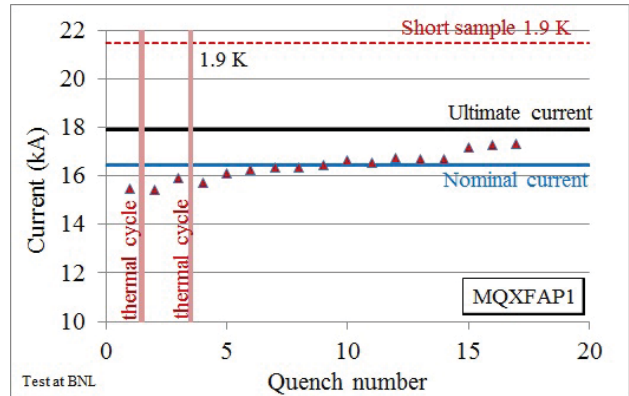
Fig. 3.17: Training of the quadrupole prototype MQXFAP1.

Having replaced the faulty coil, the magnet was reassembled in the configuration called MQXFAP1b. This magnet performance (see Fig. 3.18) was limited in performance by coil P03 previously tested in MQXFAP1 (see Table II). That coil had four consecutive quenches just around nominal in MQXFAP1, but then reached 17 kA without quench. In the second assembly, the training to ultimate was fast but erratic, and finally the magnet reached only 13 kA at 20 A/s. Moreover, it quenched when the current was stopped on a plateau even below 12 kA. All quenches were in coil P03. As for the case of MQXFS3, at the moment of writing we have no clear justification of the lack of performance of this prototype. Investigations of the mechanical properties of the limiting coil is in progress.
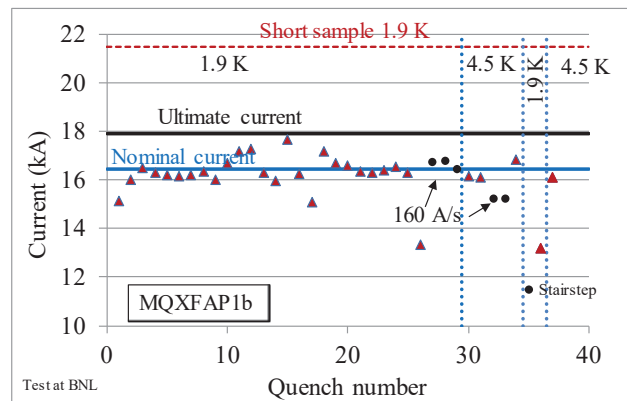
Fig. 3.18: Training of the quadrupole prototype MQXFAP1b.

The case of the second prototype MQXFP2 is treated in section 3.13. The first US-AUP preseries magnet MQXFA03 reached nominal current with 9 quenches, 8 of which in the same coil. It was trained to 200 A above nominal current, and had no retraining after the thermal cycle (see Fig. 3.19). This is the second full-size magnet to reach nominal current

and the first one with a full validation of memory, showing no need of retraining for nominal current. The magnet shall be tested to ultimate current once assembled in a cold mass with another preseries magnet. This test is particularly important since it also validated the second coil production line at BNL.
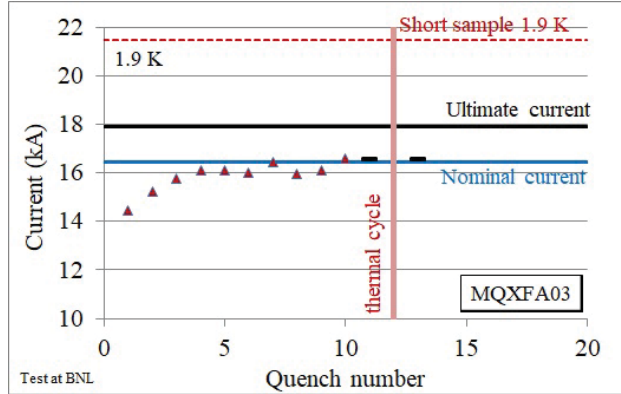
Fig. 3.19: Training of the quadrupole MQXFA03.

3.10 Design validation via power tests: field quality

As previously stated, field quality is optimized at nominal current only. For the random part, the expected field errors are based on a random displacement from the nominal position with 30 μm (one sigma) Gaussian distribution for the cable blocks; these displacements generate a distribution of multipoles used in beam dynamics simulations to confirm that particle stability is not affected. Therefore, specifications are given in terms of average and sigma, and the derivation of a tolerance band for acceptance is a non trivial passage. For the acceptance of the single magnet we set tolerances at four sigma, as shown in Fig. 3.20.

Indeed, if systematic multipoles are at the edge of the band, corrective actions are taken. To be more precise, this is a fine tuning, since there is no major change of the conductor layout, but a minor, second order modification of an optimal solution.

Fine tuning of field quality is guaranteed by two separate mechanisms for allowed and not allowed multipoles. Firstly, the redundant insulation layer in the midplane and in the pole allow a fine tuning of allowed multipoles. Moreover, magnetic shims can be inserted in the eigth slots that are used for the bladders; they allow to correct 5 units of b_3, a_3, 1 unit of b_4 and 3 units of a_4. Two multipoles can be corrected at the same time.

As shown in Fig. 3.20, the b_6 values are at the edge of the acceptance band [85]. The measurements on the first models showed a clear need of a b_6 correction of about +4 units to bring it around zero at the beginning of the production. Therefore, a 125 mm shim was removed from the midplane

and added to the pole, starting from MQXFA04 and MQXFBP2.
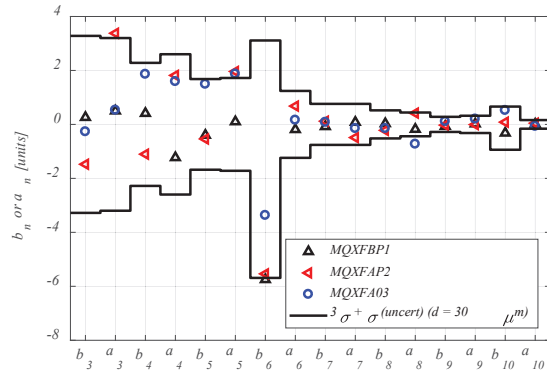
Fig. 3.20: Measured multipoles versus 4 σ range for prototypes

Some concern was present in the initial phase of the project for the non allowed multipoles. As already stated, the bladder and key structure provides a loading based on stress and not on displacement. Therefore, it was feared to have large nonallowed multipoles. The initial data on the short models confirmed large values of low order multipoles. The magnetic shimming strategy was succesfully tested to correct non allowed multipoles in all short models [85]. At the same time, the strength of the high order correctors was doubled to cope with larger errors (see also section 8.4). The data relative to a more mature part of the production revealed a much better level of field quality as shown in Fig. 3.20, namely the first results were due to the early phase of coil production and not to the assembly procedure. However, magnetic shimming has been tested on the short models to validate and acquire experience with the procedure. The four configurations tested are shown in Fig. 3.21, and the good agreement between the measured and expected correction of low order non allowed multipoles are given in Table III. Finally, one observes a very good correlation between the measurements after coil pack assembly, after loading, and at 1.9 K. This proves that the coil pack already contains all the information about the final field quality, allowing to have a precious early indicator of any anomaly in field quality [85].
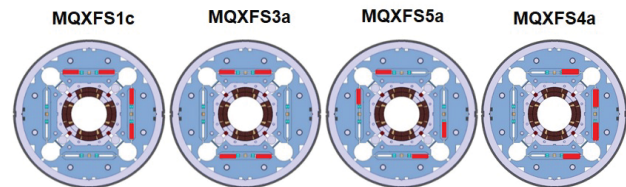
Fig. 3.21: Magnetic shimming adopted on short models

Table III Computed vs measured impact of magnetic shimming on short models

	Computed	Measured
MQXFS1c	$\Delta b_3=4.22$	$\Delta b_3=3.51$
	$\Delta a_3=-4.24$	$\Delta a_3=-3.92$
MQXFS3a	$\Delta b_4=-2.88$	$\Delta b_4=-2.55$
MQXFS5a	$\Delta a_4=0.84$	$\Delta a_4=0.71$
MQXFS3a	$\Delta b_3=3.42$	$\Delta b_3=3.30$

3.11 Design validation via power tests: protection

The protection strategy has been validated on short models without energy extraction [86], and on US prototypes with energy extraction [87]. The simultaneous use of CLIQ and quench heaters gives a quench load (from quench detection) of 27 to 29 MIITs at current ranging between nominal and ultimate (see Fig. 3.22). This corresponds to hotspot temperatures of 260 Cº to 290 Cº. In case of CLIQ failure, one has about 3.5 additional MIITs, corresponding to about additional 50º. The case of failure of one heater circuit is equal to the nominal case if CLIQ is not failing, since the CLIQ mechanism dominates over the second heater circuit.
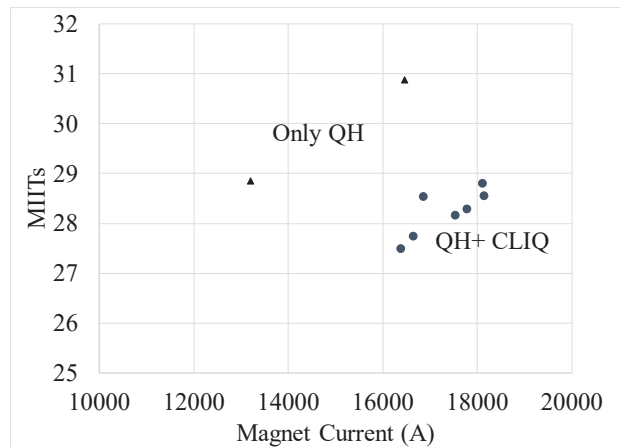
Fig. 3.22: MIITs vs current for different protection strategies

3.12 Design changes

Three main changes were carried out since the beginning of the project:

- The keystone angle of the cable has been lowered from 0.55º to 0.40º to reduce the degradation of the PIT conductor during cabling. All coils of short model MQXFS1 and one coil of the first US prototype MQXFAP1 have this initial coil geometry [88].
- The magnet length has been increased by 5% to lower the loadline fraction from 0.82 to 0.77. The initial target was to have a loadline fraction well below 0.80, but few percent were lost due to 3D effects in the coil heads and saturations, that were

neglcted in the initial conceptual design based on scaling laws. Moreover, the specification on the conductor critical current at 15 T, 4.22 K, was lowered by 10% from the intial value of 1407 A/mm^2 to 1283 A/mm^2 to mitigate the rejection risk during the strand production. This increased by another 3% the loadline fraction. Therefore, the magnet length was increased from 4.0 m to 4.2 m for MQXFA, and from 6.8 to 7.15 m for the MQXFB, to lower the operational gradient from 140 T/m to 132.6 T/m. At the time of the change, the first prototype coils in the US were already being manufactured and therefore the first US prototpye MQXFAP1 has 4.0-m-long coils. All the other prototypes coils (CERN and US) have final length.

- A 0.125-mm-thick shim has been moved from the coil midplane to the pole to increase b_6 by 5 units, as described in the previous section.

3.13 Setbacks and open issues

The short model and prototype phases had three understood setbacks. As said in section 3.9, the first prototype MQXFAP1 had a double short between a coil and a quench heater, which allowed excessive current flowing through the heater during quench; as a consequence, one coil was lost. A cause of this incident was found in the poor quality impregnation of that coil, that was among the first prototype coils and used a new insulation fabric.

The second prototype MQXFAP2 had a non-conforming Al shell without fillet radius at some corners, provoking high stress concentration and eventually a complete breakage of the shell during test. Nevertheless, the magnet reached 14 kA – a remarkable value considering the missing component in the mechanical structure. After this incident, the design of the cut-out in the Al shells was modified introducing larger radii.

The fifth short model MQXFS6 had non conforming RRR in two coils (75 compared to the specification of >100); this is believed to be the reason for the limited preformance of the magnet, barely reaching nominal current at 1.9 K. On the other hand, it must be pointed out that we have coils with RRR ranging between 80 and 95 that reached performance.

As reported in Section 3.10, we have two more cases of limitations in performance, with strong traces of reverse behaviour (MQXFS3 and MQXFAP1b) for which we have no explanation. This is the main open issue for MQXF at the moment of writing.

3.13 Timeline and schedule

The main milestones of the quadrupole development are the followings, including the under LARP.

- 2005: Design of a 90 mm aperture Nb_3Sn quadrupole TQ;
- 2007-2009: Test of the collar (TQC) and of the bladder and keys (TQS) short models;
- 2007: Design of the 90 mm aperture Nb_3Sn 4-m-long quadrupole LQ;
- 2010-2012: Test of three 3.7-m-long quadrupole LQ;
- October 2011: Beginning of the HL-LHC design study;
- 2007: Design of a 120 mm aperture Nb_3Sn quadrupole HQ;
- 2010-2012: Test of three HQ short models ;
- July 2012: Selection of triplet aperture of 150 mm;
- January 2013: Beginning of short MQXF coil manufacturing by FNAL and BNL;
- January 2014: Beginning of short MQXF coil manufacturing by CERN;
- March 2015: Beginning of long coil manufacturing by FNAL and BNL;
- March 2016: Beginning of long coil manufacturing by CERN;
- March 2016: Test of first short model MQXFS1;
- October 2016: Test of second short model MQXFS3;
- July 2017: Test of third short model MQXFS5;
- August 2017-February 2018: Test of the first prototype MQXFAP1;
- July 2018: Test of fourth short model MQXFS4;
- March 2019: Test of fifth short model MQXFS6;
- August 2019: Test of the second prototype MQXFAP2;
- December 2019: Test of the first preseries magnet MQXFA03;

US-AUP shall build 20 magnets, plus the first magnets built within LARP, and CERN shall build 12 magnets. A production line of one winding machine, one reaction oven and one impregnation system can produce coil in about 5 months, with a maximum rate of one coil per 3 weeks. Accounting for vacations and shut downs of tooling, and 5 coils per magnet, one can reach a rate of three magnets per year. A similar rate is assumed in the US, where 4.5 coils per magnet are assumed, and two production lines are operational: one at FNAL and one at BNL. Coil manufacturing is driving the magnet schedule production rate. Magnet assembly is done in 3 months, giving a total of 11 months for manufacturing one magnet.

4. The separation dipole

4.1 Accelerator requirements

The separation dipole D1 is a single aperture magnet with 150-mm-diameter bore and 35 T·m nominal integrated field. The magnet function is to increase the distance of the counter-rotating beams from zero (as it is in the experiments) to 192 mm (as it is in the LHC arcs), over the ~65 m distance between D1 and D2. The magnet is individually powered and ramps proportionally to the LHC energy from 450 GeV to 7 TeV. Field quality requirements are set at 7 TeV energy, with all multipoles at reference radius of 50 mm below 1 unit with the expection of b_3, for which a larger tolerance of 3 units is accepted. No requirements are given on the saturation of the main dipolar component that can be compensated via the power converter. No requirements are given on the field quality at injection as for all the interaction region magnets. The most exposed part of the magnet have to resist to 15 MGy dose over the HL-LHC lifetime.

4.2 Design features

The integrated field is realized via a 5.6 T nominal field over a 6.2 m magnetic length [37], produced by a 15-mm-width Nb-Ti coil that reuses the cable of the main LHC dipole, outer layer (see Fig. 4.1). We refer to the existing literature for the properties of the strand, of the cable and of the insulation. As previously stated, at nominal current the magnet operates at a loadline fraction of 0.77.
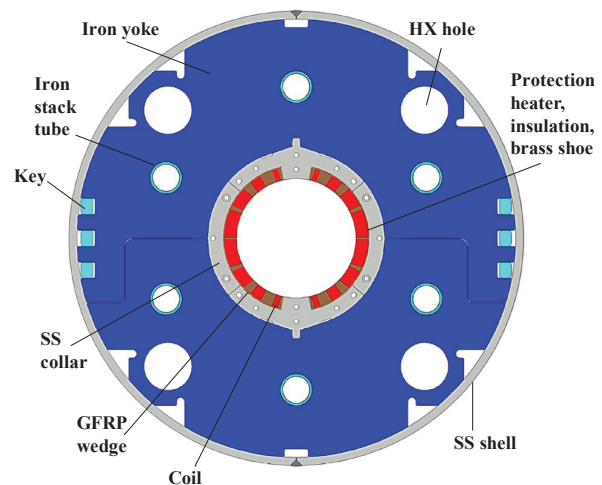
Fig. 4.1: Cross-section of the separation dipole.

The coil has four blocks : three would have been enough to satifsfy the field quality requirements, but four blocks give a larger flexibilty to make fine tuning of the multipoles. There are 15 turns in the first block, 10 in the second, 4 in the third and 4 in the fourth. As in the RHIC dipole design

[89] and in MQXA quadrupole design [18], the mechanical structure is based on iron yoke laminations with three keys on each side. 10-mm-thin spacers are used to place the iron as close as possible to the coil, maximizing the its contribution to the main field. Contrary to RHIC dipole, the spacers are not in fiberglass but in stainless steel ; they are called collars even though they are not active part of the mechanical structure.

The main challenge of this magnet is the large accumulation of stress in the midplane due to electromagnetic forces. As quoted in section 2, one has 100 MPa in the midplane, that is about twice the value of the LHC main dipole and approximately the same as in the Nb$_3$Sn HL-LHC magnets. This is an unprecedented value for Nb-Ti accelerator dipoles.

The second main challenge of the magnet is achieving the field quality target. The saturation has a strong effect not only on the main component, but also on the multipoles [36,37]. Thanks to the iron shape optimization, the variation of b_3 during the ramp is reduced to 20 units ; however, coil geometry is set to minimize b_3 at nominal current.

An additional issue is that for the 2-m-long model the ratio between lenght and aperture is such that a 3D computation of the full magnet is needed even for the field quality modeling in the straight part [40,41]. So field quality extrapolation from 2-m-long models to 6-m-long prototypes is not straightforward and must be done with proper numerical tools.

Protection is obtained by the same technology as in the LHC main magnets, i.e. quench heaters on the outer radius of the coil. A maximum hotspot temperature of 300 K is set as a limit, including the case of one heater failure [36,37,43]. The energy extraction option was discared in the initial phase of the design for cost reasons.

4.3 Design validation via power tests

KEK planned for manufacturing two short models and one prototype, plus 4 series and 2 spare magnets. Prior to the short model construction, a mechanical model was done to validate the coil size, the shimming to reach nominal precompression, and the assembly and the yoking procedures.

The first short model MBXFS1 reached nominal current after 15 quenches [38], and had erratic behaviour between nominal and ultimate current (see Fig. 4.2). The short model azimuthal coil size turned out to be much smaller than what needed for full preload at ultimate current. This induced a loss of preload already at current values between 6 and 8 kA (see Fig. 4.3). The coil had also an insufficient support of the ends, and after the first test a movement up to 4 mm in the coil turns towards the magnet aperture was observed in the coil heads.

The second assembly MBXFS1b included a 0.8-mm-thick shim in the midplane to increase the precompression. The magnet reached performance: nominal current was reached after two quenches, and ultimate current after five quenches (see Fig. 4.2, after the vertical blue line). After thermal cycle no retraining was needed for nominal current, and two quenches for ultimate current [39]. The magnet showed pole unloading in the straight part above 12 kA, but was able to train up to 13 kA (see Figs. 4.2 and 4.3).
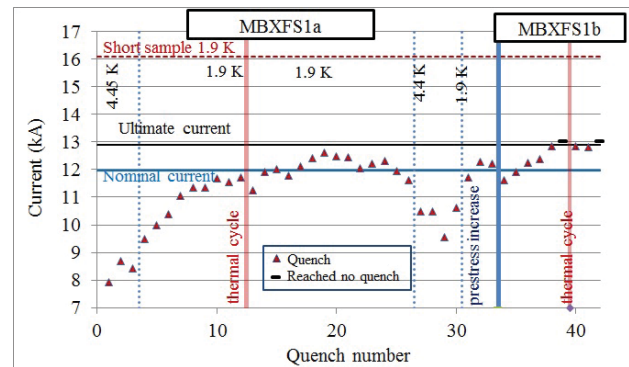
Fig. 4.2: Training of the first separation dipole short model.
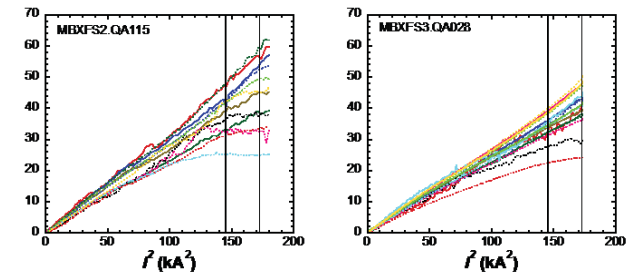
Fig. 4.3: Strain gauge measurement of pole unloading during the MBXFS1 and MBXFS1b powering.

In the second short model [42], wedges were enlarged by a total of 1.2 mm to have a larger azimuthal coil size aiming at full precompression at ultimate current. Moreover, there was an iteration on the iron yoke (see next section) and consequently on the coil cross section. The magnet reached performance (see Fig. 4.4): nominal current was reached after 7 quenches, and ultimate current after 12 quenches. After thermal cycle, one quench was required for nominal and about ten for ultimate. Strain gauges measurements confirmed that this magnet had a sufficient precompression in the straight part to avoid coil unloading at ultimate current, as planned (see Fig. 4.3).

After the second short model results, it was proposed to manufacture an additional short model to validate the performance and field quality reproducibility. The third short model, manufactured as a perfect copy of the second one, reached nominal current with one quench, and ultimate current with 20 quenches (see Fig. 4.5). It was tested at

4.5 K, showing the ability of operating above nominal. Memory proved to be very good, with no quenches to nominal after thermal cycle and three quenches to ultimate. Strain gauges showed also in this case full precompression up to ultimate current (see Fig. 4.3). These results validated the design, allowing to start the construction of the prototype, that is ongoing in Hitachi at the time of writing.

Field quality was measured to be in line with the expectations. The measurements of b_3 versus the OPERA model is shown in Fig. 4.6 for the short model MBXFS2.
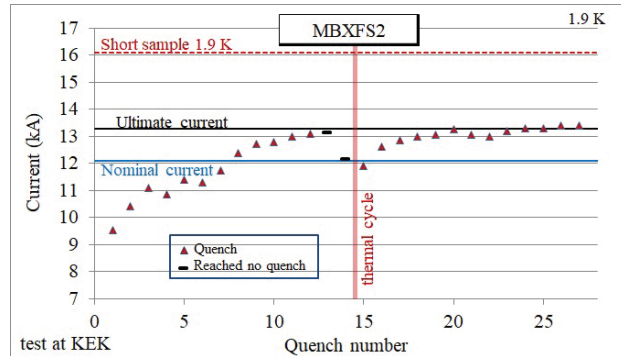
Fig. 4.4: Training of the second separation dipole short model.
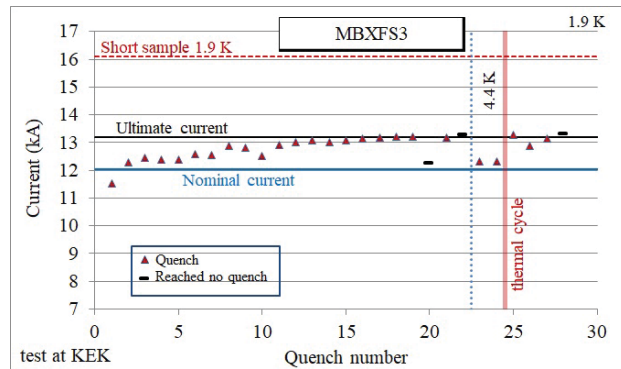
Fig. 4.5: Training of the third separation dipole short model.
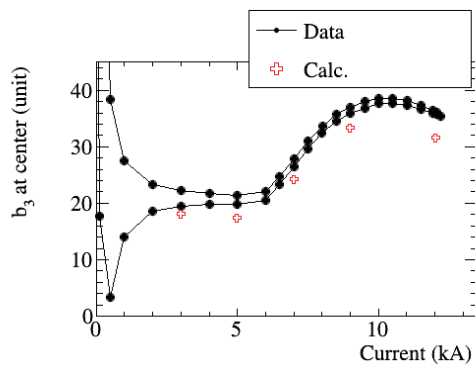
Fig. 4.6: Measured versus modeled b_3 along the ramp in the second short model.

4.4 Design changes

The design went through the following iterations [43].

- After the mechanical model, a change in the shape of the collar spacers was done to improve the alignment of the assembly (see the change from the triangular shape of the collar in Fig. 4.7 to the alignment notch in Fig. 4.1).
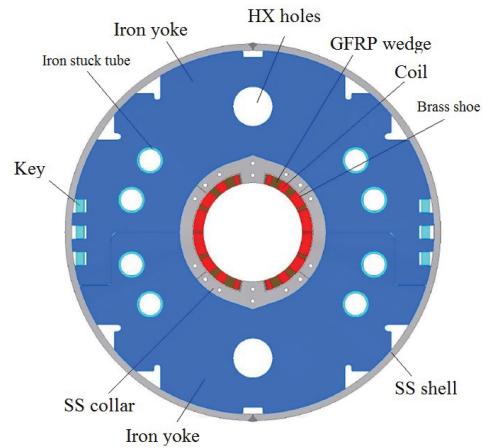
Fig. 4.7: First cross-section of the separation dipole.

- The position of the cooling holes was initially set to 90º and 270º (see Fig. 4.7); it was later moved to 45º, 135º, 225º and 315º (as in the triplet, see Fig. 4.1) to account for the constraints due to interconnections.

- There has been a change of cross-section from MBXFS1 to MBXFS2 to better optimize field quality, both for the correction of the 3D effects coupled with saturation, that were ingored in the first layout, and for taking into account of the new geomtry of the iron holes.

- The nominal magnetic field was increased by 2% to reduce the total length of the magnet below 6.5 m, thus allowing vertical test in KEK. Without this reduction of length the magnet would have not fitted the test station and the cost for an upgrade would have been not acceptable for the project.

- The quench heaters were initially a simple strip covering one coil block; this design proved to be not enough efficient to quench the coil. It has been replaced by two strips, zigzaging between three blocks of the magnet, and with copper coating in the transition between the blocks to reduce to total resistance of the strip (see Fig. 4.8). With this design, at nominal current the coil is quenched within 10 ms.

4.3 Setbacks and open issues

The most relevant issue in this magnet is the control of azimuthal prestress in the straight part and in the coil ends. We had one setback in performance for the first magnet assembly. The origin is clearly due to precompression in the coil, but it was not possible to state if the cause was the lack of prestress in the straight part or the lack of support in the coil end. As stated in the previous paragraph, movements of up to 4 mm of the coil in the ends towards the magnet aperture were observed in MBXFS1. Both the second and third short model showed similar movements, but with much smaller amplitude (less than 1 mm). This seems not to limit the performance, but is a source of concern for the prototype and series magnets. On the other hand, MBXFS2 data show that a partial unload around nominal current in the straight part does not prevent reaching ultimate current.
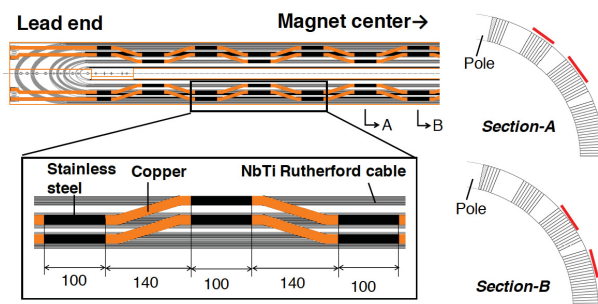
Fig. 4.8: Geometry of the quench heaters.

The other challenge of this magnet is the control of field quality, and mainly the low order harmonics at nominal current. The second and third model have an integral b_3 of about 40 units (see Fig. 4.6). Half of them are expected to disappear in the prototype, due to the dilution of end effects and to the reduciton of saturation coupling with coil ends. The other half, whose origin is well understood, shall be corrected with a fine tuning of the wedges in the prototype. One should finally land on the ±3 units target allowed by beam dynamics. The way is long, but an additional iteration could be done (if needed) between the prototype and the series.

4.4 Timeline and schedule

The main milestones of the D1 development are the followings:
- October 2011: Beginning of the design study;
- July 2013: Selection of bore aperture;
- April 2014: Beginning of coil manufacturing of the short model (practice coil);
- Mid 2015: Mechanical model and iteration on the collars shape;
- April 2016: Test of the first short model;

- February 2017: Test of the second assembly of the first short model;
- October 2018: Test of the second short model;
- May 2019: Contract for prototype and series;
- September 2019: Test of the third short model;
- January 2020: Beginning of prototype winding.

The prototype and the six series magnets shall be built at Hitachi with an industrial contract steered and financed by KEK. The schedule is driven by the funding profile, with a rate of two magnets per year.

5. The recombination dipole

5.1 Accelerator requirements

The separation dipole D2 is a double aperture dipole with 105-mm-diameter bore and a 35 T·m nominal integrated field. The magnet function is to decrease the distance of the counter-rotating beams from 192 mm (as it is in the LHC arcs) to zero (as it is in D1), over the ~65 m distance between D1 and D2. The two apertures are powered in series, with fields in the same vertical direction. The magnet is individually powered and ramps proportionally to the LHC energy from 450 GeV to 7 TeV. Field quality requirements are set at 7 TeV energy, with all multipoles at reference radius of 35 mm below 1 unit with the expection of b_3, for which a larger tolerance of 3 units is accepted. No requirements are given on the saturation of the main dipolar component that can be compensated via the power converter. No requirements are given on the field quality at injection as for all the interaction region magnets. The most exposed part of the magnet have to resist to 15 MGy dose over the HL-LHC lifetime.

5.2 Design features

The integrated field is realized via a 4.5 T nominal field over a 7.8 m magnetic length, produced by a 15-mm-width Nb-Ti coil that reuses the cable of the main LHC dipole, outer layer, as in D1 (see Fig. 5.1). We refer to the existing literature for the properties of the strand, of the cable and of the insulation.

This design [44,45,46] was also selected since INFN Genova and Milano had acquired experience with the FAIR SIS-300 fast-ramped dipole construction [90]. This dipole has very similar parameters, namely a 4.5 T field, a 100 mm aperture, and a one layer Nb-Ti coil with the same LHC dipole outer cable. The main difference is that SIS 300 dipole is slightly curved, and it makes use of a strand with finer filaments (3 μm instead of 6/7 μm as in the LHC) to minimize the losses during fast ramp (up to 1 T/s).
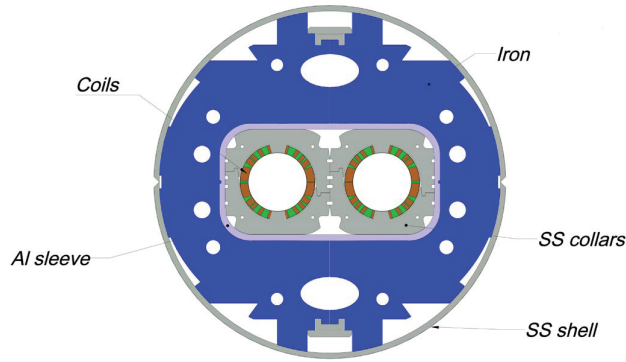
Fig. 5.1: Cross-section of the recombination dipole D2.

In D2 recombination dipole, the main additional challenge with respect to SIS 300 is the double aperture, giving a non-negligible magnetic cross-talk between apertures [44]. To be more quantitative, the b_2 component at 35 mm reference radius is of the order of 2% of the dipolar field (200 units). To reduce this cross-talk, the coils are left-right asymmetric (see Fig. 5.2) as proposed for the D2 dipole in [48].

The iron is far away from the coil, allowing self-supporting stainless steel collars. The limit in the bore field is set by the targets on the allowed multipoles; above 4.5 T the dependence of b_3 on current becomes very steep, due to iron saturation, and therefore it becomes very difficult to control. Note that with respect to D1, having the same cable and a similar current, ~1 T is lost due to the cross-talk of the apertures (contrary to LHC dipoles, fields point in the same direction) and due to the lower impact of the iron. Last but not least, differently to the LHC dipoles, independent collared apertures were selected. This allows larger flexibility for such a small production, and an easier collaring procedure, with a moderate cost increase. With these design choices, the magnet operates at a loadline fraction of 0.68, i.e., slightly below the initial target of 0.70.
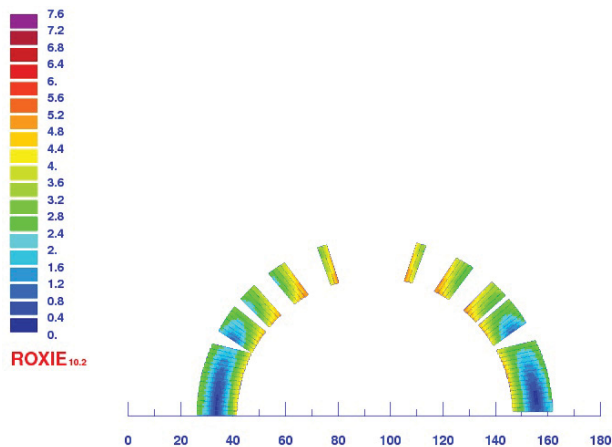
Fig. 5.2: Cross-section of the coil of the recombination dipole D2.

The coil has five blocks (see Fig. 5.2). Three would have been enough to satifsfy the field quality requirements, and four were considered to be necessary to have enough free parameters to steer field quality, as for the D1. A main challenge was to find an asymmetric coil with the same number of turns per block on the right and on the left part, to avoid complexity in the coil heads. This challenging optimization problem was solved with five blocks, and was adopted for the short model [44,45]. Later, a four block solution was found with a clever optimization algorithm, but the model was already engineered and the redundant wedge was deemed to provide an additional free parameter for fine tuning of field quality, with a minor extra cost.

There are 15 turns in the first block, 6 in the second, 4 in the third, 4 in the fourth and 2 in the fifth. Collars have a 25 mm thickness. The level of stress is similar to the LHC dipoles (see Fig. 2.5), so it is a challenging value in terms of precompression, but not at the level of the D1 previously discussed.

A novel solution is used to manage to repulsive force between the apertures : an Al sleeve is assembled at room temperature around the two apertures, with a 0.1 mm radial gap, and thanks to the larger thermal contraction it locks and aligns the two apertures at 1.9 K. The sleeves, 10-mm-thick, are warmed up to ease the assembly, and after test can be easily removed.

As in D1, the main challenge of the magnet is achieving the field quality target. All the optimization relies on the compensation of the two apertures and on the impact of the iron. Just to give the order of magnitude of the problem, the single aperture has 170 units b_3 ; when the two apertures are put together, b_3 moves to 80 units. When the iron is added, b_3 finally falls on the ±3 units range. So a compensation better than 95% is required. Field quality optimization relies on this delicate balance between coil cross-talk and iron shape. The good side is that these effects can be measured at room temperature. Moreover, the iron saturation is not so dramatic as in D1, as the field is 1 T smaller and the iron is 15 mm more distant from the coils.

Protection is guaranteed by the same technologies as in the LHC main magnets, i.e. quench heaters on the outer radius of the coil. A maximum hotspot temperarure of 300 K is set as a limit, including the case of one heater failure. The energy extraction option was discared in the initial phase of the design for reasons of cost. The heaters cover three out of the five coil blocks, allowing to quenching the magnet within 10-20 ms from quench detection at nominal current.

5.3 Design validation via power tests

INFN-Genova, in charge of the design, engineering and construction of the model, assigned the tender for the magnet manufacturing to ASG Superconductors (Italy). The program

includes one double aperture short model, one prototype, four series magnets and two spares. The short model test showed that the magnet was limited in one coil of one aperture at 10 kA, i.e. about 2 kA lower than nominal current (see Fig. 5.3). After disconnecting the faulty aperture, the other one reached nominal current without quenches, and ultimate current with two quenches. Note that for this single aperture test – not in the baseline - a fine tuning of the nominal/ultimate current concept was done to have the same loadline fraction as the double aperture magnet (see Fig. 5.3).
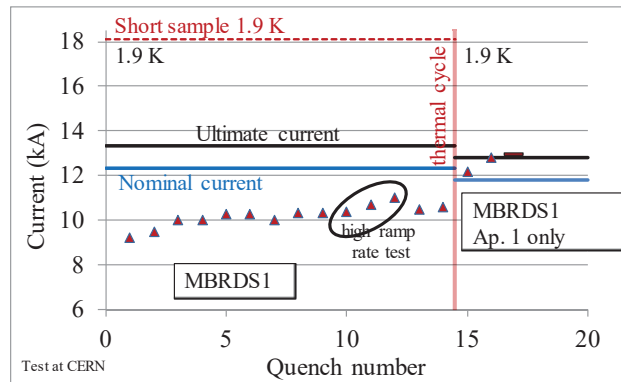
Fig. 5.3: Training of the recombination dipole short model.

The first test had no magnetic measurements at 1.9 K, and therefore the saturation component could not be validated with power tests. On the other hand, room temperature measurements were giving relevant information (see Table IV). The optimization of field quality was proven within 10 units for b_3 and b_5. The missing part towards the target of ± 3 units (for b_3) and ± 1 unit (for b_5) was found to be due to a missing shim of 0.125 mm in the midplane.

Table IV. Magnetic measurements at room temperature of short model, straight part, with and without yoke. Multipoles given at 35 mm reference radius.

	Without yoke		With yoke	
Multipole	Ap. 1	Ap. 2	Ap. 1	Ap. 2
b2	209	-205	12.79	-9.41
b3	81.0	81.8	9.17	10.0
b4	-8.97	10.3	2.06	-0.38
b5	-0.01	3.06	6.95	9.30
b6	-2.96	2.98	-1.72	1.68
b7	-0.34	0.31	-0.31	0.00
a2	1.03	2.40	2.43	4.03
a3	-2.84	-2.85	-2.39	-1.83
a4	1.16	-0.13	0.95	-0.62
a5	2.42	1.59	1.67	1.40
a6	0.57	1.93	0.46	1.63
a7	1.67	1.64	1.02	1.14

The strain gauges measurements were also not conclusive, so we have no identification of the prestress level and of the coil

unloading. The quench heaters were not installed and energy extraction was used, so no proof was given for the protection strategy. A fifth coil was build to replace the faulty one, the third aperture was collared in December 2019 and the second test was carried out in February 2020.

5.4 Design changes

There were few iterations on the magnet design. The collars were initially separated from the nose (see Fig. 5.4); in the third aperture [46] it has been decided to include them in the collars to reduce the piling-up of tolerances, and to minimize the possilbity of misplacement during assembly. The second iteration was done to optimize the area around the layer jump, that caused considerable issues in this magnet (see next section). The third iteration was done on the iron shape; an ellitical shape was adopted in the short model to reduce the saturation component of b_3. This required an additional component for the cold mass assembly in the circular stainless steel shell (see the fillers in orange, Fig. 5.4). For the prototype and series, it has been decided to remove this component to reduce the cost and ease the assembly, and adopt the shape shown in Fig. 5.1. The circular hole for the heat exchanger, present in a previous cross-section not shown in this paper, was replaced in a very early phase of the project with an elliptical one. The main reason is that the cooling scheme was changed from heat exchanger to direct cooling, and therefore a 200 cm^2 of free cross-section in the magnet was needed for heat extraction. Part of this surface was obtained through the elliptical shape of the hole.
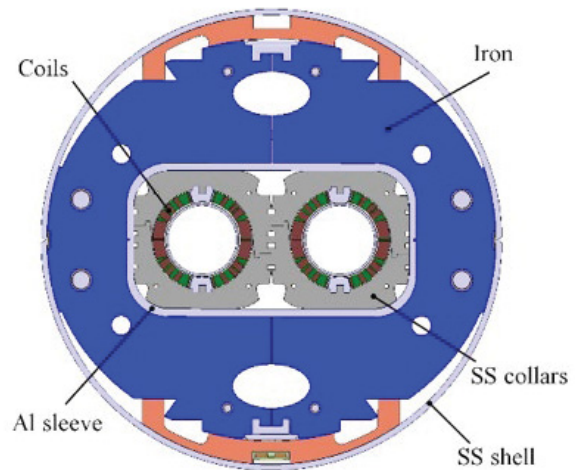
Fig. 5.4: First cross-section of the recombination dipole D2.

5.5 Setbacks and open issues

The most critical issue for the magnet performance has been the design and the assembly of the layer jump that goes to the connection leads. The cable is kept in place via a G11

box as in the LHC main dipole, but there is no outer layer; therefore this box has to go through a cut in the collars that weakens the structure in the connection side, just before the coil heads. The first aperture had a short in this region after collaring; visual inspection revelaed no trace of the short, but after an insulation reinforcement and a second collaring the short disappeared. The same aperture, and coil, was limiting performance in power test at 1.9 K (see Fig. 5.3). After disassembly, the layer jump box was found to be broken and about half of the strands of the cable were cut during the collaring, thus justifying the severe magnet performance limitation. The third aperture, build to replace the first one, also showed a short circuit that was located at the cable exit, at the coil protection sheet. An iteration on the design of this region is in progress and will be implemented in the prototype.

The second issue that was found was an excess of prestress in the coil heads, fracturing or breaking the end spacers. In the third aperture the first end spacer had a breakage leaving unprotected 5 mm of cable. The region was repaired by filling with charged stycast. For the second assembly of the short model third aperture, a preassembly with Fuji paper has been used to determine the level of prestress in the coil heads and avoid these issues.

5.4 Timeline and schedule

The main milestones of the recombination dipole development are the followings:

- April 2014: Beginning of the design study;
- September 2016: Tender for the short model awarded to ASG Superconductors with contract start in November 2016;
- March 2018: beginning of coil winding for the short model;
- October 2018: Tender for the prototype with option on the series attributed to ASG, with contract start in March 2019;
- February 2019: test of the short model, including disconnection of the faulty aperture;
- Summer 2019: fabrication of the third aperture of the short model;
- January 2020: tooling preparation for prototype.

The rate assumed for the schedule is a very conservative 3 magnets per year at full speed. This is done via one coil production line. Coil construction takes 3 months, 2 months for collaring and 2 for yoking. The cold mass is done at CERN, where the orbit correctors based on CCT technology (see Section 7) are included. Due to the manget length, it was not possible to find a station to test it vertically. This causes a very long feedback loop in case of issues during the test, namely one year from test to test in case of disassembly up to the level of the collared coil.

6. The nested dipole correctors

6.1 Accelerator requirements

The nested orbit correctors are single aperture dipoles with 150-mm-diameter bore and a 2.5/4.5 T·m nominal integrated field, both in horizontal and vertical direction. The magnet has two different lengths; the magnet MCBXFB is 1.5 m long, has 2.5 T·m integrated field, and has to be assembled in the Q2a and Q2b cold masses (one per cold mass, see Fig. 2.1). The main function of these magnets is the correction of the misalignment of the triplet. The magnet MCBXFA is 2.5 m long, for a 4.5 T·m integrated field, and has to be assembled in the corrector package cold mass. Besides correcting the orbit error due to the triplet alignment, it also contributes to open the crossing angle. Each aperture is individually powered, and the magnet shall operate at any combination vertical/horizontal dipole, with both directions of the field. Field quality requirements are set at 7 TeV energy, with all multipoles at reference radius of 50 mm below 5 units with the exception of b_3, for which a larger tolerance of 20 units is accepted. No requirements are given on the saturation of the main dipolar component that can be compensated via the power converter. No requirements are given on the field quality at injection as for all the interaction region magnets. There are three magnets per IP side, each one having two circuits, for a total number of 24 power converters. To optimize the cost, 2 kA is set as a maximum value for the nominal current. The most exposed part of the magnet have to resist to 30 MGy dose over the HL-LHC lifetime

6.2 Design features

In order to satisfy the constraint on the current, a double layer coil based on a small Rutherford cable was used, namely a 4.37-mm-width cable, with 18 strands and a 0.48-mm-diameter wire. The wire was already used for the cable of MQM and MQY in the LHC [1]. The cable was specially developed in the framework of the S-LHC project for an upgrade of the orbit corrector of the triplet.

With such a large aperture and such a small width cable, 70 to 100 turns are needed for each layer (see Fig. 6.1 and 6.2, and Table I) and therefore the option of an impregnated coil was taken. The same technology of Nb3Sn was adopted, namely a fiberglass insulation and CTD-101K resin [49,50,51].

The vertical dipole coil has 3 blocks (inner layer) and 3 blocks (outer layer), for a total of 140 turns. The horizontal dipole coil has also 3 blocks (inner layer) and 3 blocks (outer layer), for a total of 191 turns (see Fig. 6.1). A large contribution to the field comes from the iron, namely 34% for the inner layer and 64% for the outer layer. Therefore the current density in the outer dipole is about 15% smaller than

in the inner dipole. However, current densities are of the order of 300 A/mm², i.e. 30% lower than in the main HL-LHC IR magnets (see Fig. 2.5).
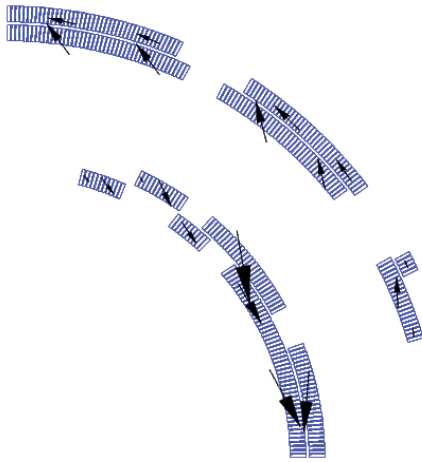
Fig. 6.1: Cross-section of the nested dipole corrector coil, and electromagnetic forces with nominal current in both dipoles (one quarter shown).
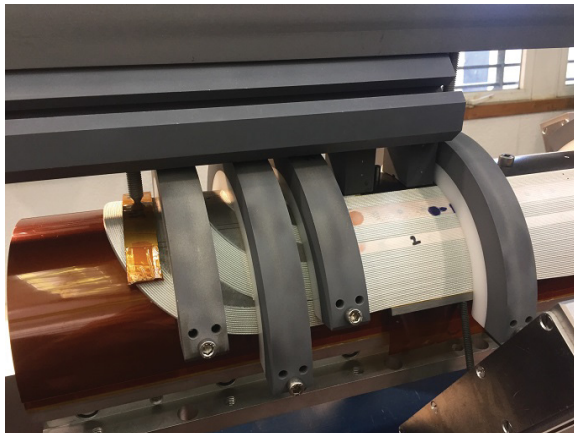
Fig. 6.2: Coil head during winding.

Each coil provides a bore field of 2.15 / 2.26 T (vertical/horizontal). In single dipole configuration, the peak field is 2.54/2.65 T (vertical/horizontal); in combined mode, a bore field of 3.12 T field with an inclination of 45º is provided, with a peak field of 4.3 T in the inner layer of the vertical coil. This corresponds to a loadline fraction of 0.51 fitting the guidelines given in Section 2. In single powering mode, there is a 25 MPa/40 MPa accumulated stress in the midplane of the inner/outer dipole. Therefore the required precompression to avoid pole unload at nominal current is not critical. When both dipoles are powered the precompression required to avoid any coil movement increases from 25 to 45 MPa for the inner dipole.

The first non trivial element of the nested corrector design is that when both dipoles are powered, a force directed towards the bore is applied to the coil pole of the inner dipole (see Fig. 6.1). Neglecting the influence of the inner field, and only considering the outer horizontal field acting on the current line of the inner dipole coil (see Fig. 6.3), one can give a first order estimate of the shear stress on the pole

$$\sigma_s \sim jBh \ \cos\frac{\pi}{3} \qquad (5)$$

where h is the length of the cable block on the pole, and therefore for a 310 A/mm² current density, 2.26 T horizontal field and $h\sim$10 mm coil width, one gets ~10 MPa. Using the map of electromagnetic forces computed on the actual cross-section (see Fig. 6.1), one finds a maximum shear stress between the coil and the pole/wedge of 10 MPa. This shear stress is balanced by a coil precompression at 1.9 K of 80 MPa, providing a residual compressive azimuthal stress of 35 MPa in any operational conditions. This compressive stress prevents coil displacements towards the bore when both dipoles are powered. In the initial design, a radial gap of 3 mm was left between the inner bore and the coil to allow sliding a tube to prevent inward movements of the coil. Therefore, the inner coil radius is 78 mm and not 75 mm. The option of the inner support tube was abandoned in an early phase of the project, considering that the coil preload was suffient to avoid inward movements of the coil.
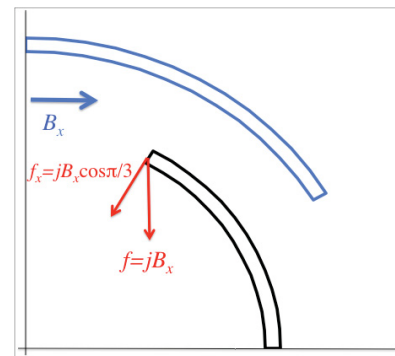
Fig. 6.3: Electromagnetic forces induced by outer dipole acting on the inner dipole coil (neglecting inner dipole field effect).

A second non trivial element of the design is that when both dipoles are powered at nominal curernt there is a 140 kN·m/m torque. To manage this large torque a double collared structure with a mechanical lock between the horizontal and the vertical apertures has been developed (see Fig. 6.4). Collars have a 25 mm thickness, and the mechanical lock is present on the straight part of the magnet; there is a 1 mm nominal gap between the vertical dipole coil and the inner dipole collars. The coil heads have no mechanical lock. If the coil heads were free to slide, the maximum relative movement between the two layers is

0.2 mm. Coils heads are also precompressed by collars to prevent the coil motion inside the round collars used in the ends.

With respect to the mechanical design, field quality aspects are less critical. The iron is placed at 25 mm distance from the outer dipole coil, and since main field is around 2 T in each dipole direction, saturation of the transfer function is negligible for the inner dipole, and 2% for the outer dipole. The iron has four holes aligned with the heat exchangers of the triplet: these holes create an asymmetry that through iron saturation affect the multipoles (mainly b_3 and a_3, see Fig. 6.5). Since all powering configurations have to be considered, this effect cannot be considerably reduced through iron shaping. However, with this design the a_3 and b_3 fit the beam dynamics requirement of 20 units tolerance. Getting rid of the iron would give perfect field quality, but with the price of losing the iron contribution to the main field, i.e. giving a 34% larger current in the inner dipole, and 64% higher in the outer dipole. Moreover, it would increase the loadline fraction. In one word, one would need to compensate the lack of iron with a larger width cable, and this would furhter increase the operational current.
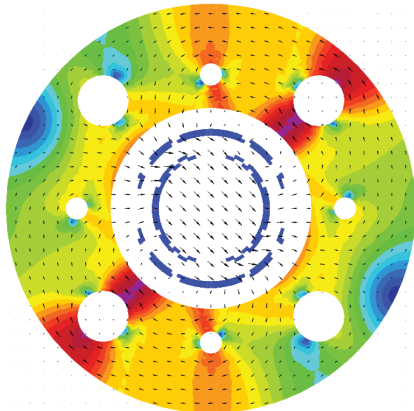
Protection is guaranteed by energy extraction, with an hotspot temperature below 250 K. Due to the large number of turns, inductance is large enough (between 50 and 200 mH for long/short and inner/outer dipole, see Table I) to require an active protection system (i.e. the magnet is not self protected). Quench heaters were initially considered, but discarded in an early phase of the project to reduce complexities in the coil manufacturing and in the magnet assembly.

6.3 Design validation via power tests

The first prototype (1.5-m-long corrector MCBXFBP1) was initially tested only with the inner dipole assembly; the magnet reached ultimate current without training (see Fig. 6.6). The outer dipole dipole was then added to the magnet asssembly, and in the final configuration the outer dipole also reached ultimate current with 11 quenches, all in the outer dipole coils. In combined powering mode, only 50% of the product between the horizontal and vertical field was reached, with all quenches in the outer dipole and localized in the coil heads.

Fig. 6.4: Cross-section of the nested dipole corrector coil
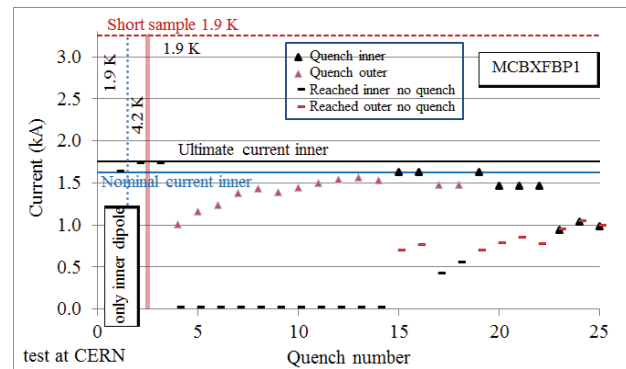
Fig. 6.6: Training of MCBXFBP1

In the second assembly the pole shims thickness was changed from 0.8 mm to 1.0 mm in the inner dipole pole to increase the precompression in the straight part. The magnet showed no retraining for individual powering, and the same limitation to 50% of the B_x B_y, with the same quench location. This phenomenology showed that the performance issue was not relative to shear stress in the inner dipole, but rather to the torque in the coil ends.

The magnet had a third assembly where ~0.6 mm of the pole shim was moved in the midplane (both for the vertical and the horozontal dipole), and prolonged up to the end of the magnet; in fact the coil size measurements gave an indication of a midplane gap of ~0.5 mm in the coil heads. In this new configuration, the magnet reached nominal current in both planes after 10-20 quenches (see Fig. 6.7).

Fig. 6.5: Field map in the iron during simultaneous powering of both dipoles at nominal field
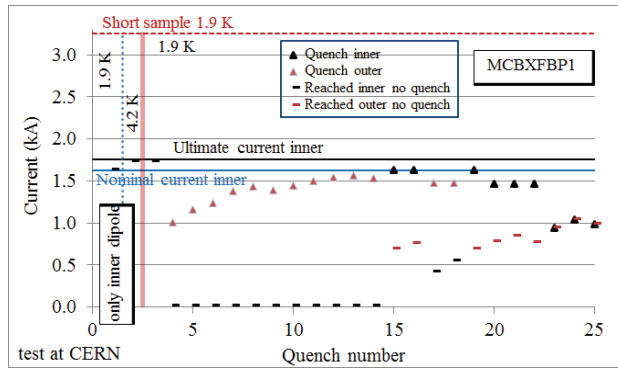
Fig. 6.7: Training of MCBXFBP1c

After this training, the could operate in the opposite quadrant (negative current in both dipoles) at nominal current. To operate in the other two quadrants, a further training of ~10 quenches was required. This training for reaching positive horizontal dipole and negative vertical (or viceversa) prevents to operate with the dipoles having the same sign. This feature should pose no limitations to operation in the accelerator; however, a larger precompression of the coil heads will be used for the second prototype to see if this issue can be overcome.

6.4 Design changes

The first version of the magnet had a single layer coil; this was providing a simpler design, at the price of a higher ladline fraction (~0.65) and operational current (~3 kA). The 2 kA limitation on power converter forced to go for a double layer design, also allowing to decrease the loadline fraction around 50% and getting more operational margin. This change was done in an early phase of the project (2015), i.e. well before the engineering phase.

The second design change concerned the position of the heat exchangers. As for the D1 (see Section 4) initially the holes for the long corrector MCBXFA were at 90º and at 270º, plus two additional at 0º and at 180º not to break the symmetry of the corrector. In 2016 was realized that the interconnection geometry imposed the alignment of heat exchanger between the triplet, the corrector package and the D1. Therefore all the heat exchanger holes were positioned at 45º, 135º, 225º and 315º as shown in Fig. 6.1.

The third change concerned the protection system. Initially simulations showed that the short magnet MCBXFB could be protected by quench propagation, without the need of energy extraction. Results of the first tests showed that quench propagation did not ensure to keep the hotspot temperature below the 300 K limit, and therefore an extraction system has been included.

6.5 Setbacks and open issues

The most critical part is the support of the coil heads. The mechanical lock is present only in the straight part, and an adequate level of precompression in the coil head has to be used to avoid training.

The precompression in the straight part was shown to be effective was effective to prevent the motion of the inner coil towards the magnet centre under the electromagntic forces. Therefore the option of an inner tube to support the coil from inside the aperture has been discarded.

6.6 Timeline and schedule

The main milestones of the canted dipole corrector development are the followings:

- July 2014: First conceptual design based on double collaring and single layer;
- June 2015: Double layer design;
- January 2016: Beginning of engineering design;
- February 2017: Mechanical model;
- September 2017: Beginning of coil winding;
- Fall 2018: Collaring of the prototype
- January 2019-August 2019: test of the first prototype with succesive iterations on the magnet assembly parameters.

7. The canted cos theta dipole correctors

7.1 Accelerator requirements

The D2 orbit correctors are double aperture dipoles with 105-mm-diameter bore and a 5 T·m nominal integrated field. The magnet function is to open the crossing angle in the interaction point, to close any possible orbit bump in the crab cavities located between D2 and Q4, and to correct the orbit error due to misalignent of the triplet. Each aperture is individually powered and settings are given by the sum of the three different fuctions carried out by this magnet. Field quality requirements are set at 7 TeV energy, with all multipoles at reference radius of 35 mm within ±5 units with the expection of b_3, for which a larger tolerance of ±20 units is accepted. No requirements are given on the saturation of the main dipolar component that can be compensated via the power converter. No requirements are given on the field quality at injection as for all the interaction region magnets. Two set of magnets are needed for each D2 : an horizontal and a vertical dipole. The most exposed part of the magnet have to resist to 6 MGy dose over the HL-LHC lifetime.

7.2 Design features

Since the two apertures can be powered in any configuration, the magnetic cross-talk cannot be compensated by asymmetric coil design as in D2. Therfore,

the field quality constraints set a limit on the maximum field, that should be not too far from the iron saturation levels. For D2 correctors, a bore field of 2.6 T has been selected, for a 1.9 m magnetic length (see Table I). As in the LHC [1], horizontal and vertical dipoles are alternatively coupled in the same magnet to reduce the cross-talk between apertures.

The initial layout was based on a standard sector coil; then it was decided to adopt a canted cos theta coil [52,53]. According to this idea [55], two tilted solenoids are wound in a metallic former, with opposite inclination (see Fig. 7.1, where the two windings are shown before assembly). When the two coils are assembled around the same aperutre, the solenoidal field is canceled and a pure dipolar field is left. The design has the advantage of requiring a very simple winding machine, and very little tooling and components for the assembly : no collars, no press, no wedges, no end spacers. On the other hand, a large fraction of the conductor is used to generate a solenoidal field that is canceled by the other winding, and there is no way of prestressing the conductor in the groove. This design was considered to be ideal for a low to intermediate field application (i.e., 2 to 4 T) as the D2 corrector, since the conductor is not a relevant part of the cost.

The loadline fraction was set to be lower than 50%, as in all correctors. This was realized, see [52,53], with a 10 turns per slot winding (see Fig. 7.2) of a 0.825-mm-diameter Nb-Ti wire (same wire of the LHC outer dipole cable). Each wire is insulated by wrapping polymide tape, for a total diameter of the insulated wire of 1 mm. The slots in the former are 2.1 mm wide times 5.2 mm deep to allow an easy but tight winding. The slots make 365 turns over the 2-m-long magnet, with a 30˚ angle with respect to the beam axis. The former material is Al, hard anodized to reinforce insulation. The two formers with opposite tilted solenoids are impregnated together with CTD-101K to ensure a mechanical stability of the coil.

The magnet has the advantage of a very low opertional current (400 A), but the drawback of a large inductance (~1 H per aperture). A maximum hotspot temperature of 200 K is set for these correctors. Protection is ensured via a dump resistor that starts a quench back thanks to the current induced in the Al former. Since the main protection mechanism is the quench back, the copper content of the wire or even the current density in the wire is not a critical parameter for protection. Indeed, this magnet design is a different paradigm with respect to cos theta and block coil magnets. A schematic cross-section of the two apertures with the iron yoke is given in Fig. 7.3.

The magnet design was developed at CERN, with the a short model and a 2-m-long prototype program. In 2018, China agreed with CERN to have the 12 series magnets as an in-kind contribution, plus a protoype, based on CERN

design. At the moment of writing the first Chinese protoype is being completed in WST (Western Technologies), X'ian.

Fig. 7.1: Two two tiltes solenoids of the short model of the canted corrector before being inserted one into the other.
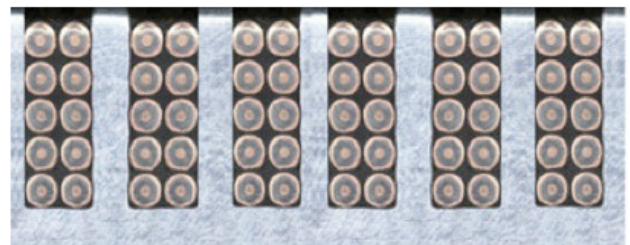
Fig. 7.2: Position of the wire in the grooves of the formers.
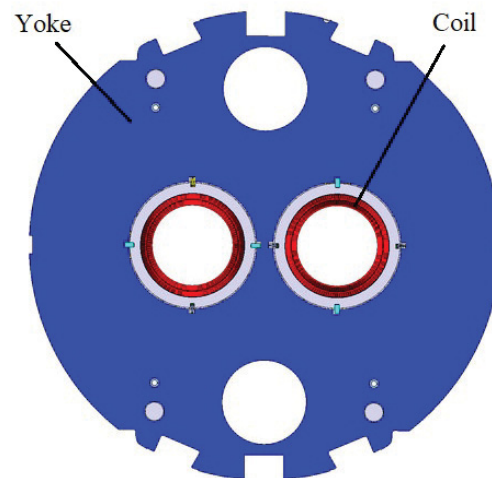
Fig. 7.3: Cross-section of the MCBRD magnet.

7.3 Design validation via power tests

Even though the D2 corrector is only 2 m long, since CERN had no previous experience in this design, it was decided to start manufacturing a double aperture 0.5-m-long model [54]. The first aperture reached nominal current without quench, and ultimate with one quench, showing perfect memory after thermal cycle. The second aperture had similar performance and was powered up to 75% of maximum current (see Fig. 7.4).
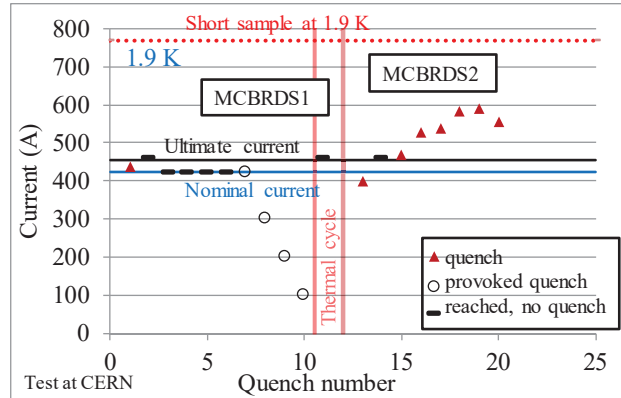
Fig. 7.4: Training performance of canted corrector short model.

Then, a full size prototype with 2-m-long coils was manufactured. The protoype second aperture had similar performance of the short model, but the first aperture required a long training [54], with 20 quenches to nominal and another 10 quenches to ultimate (see Fig. 7.5). A third aperture was manufactured to verify this training behaviour. In this test, the new aperture required three quenches to reach ultimate current, and the previously tested aperture reached ultimate wihtout retraining (see Fig. 7.5). Both apertures reached ultimate current at 4.5 K without training.
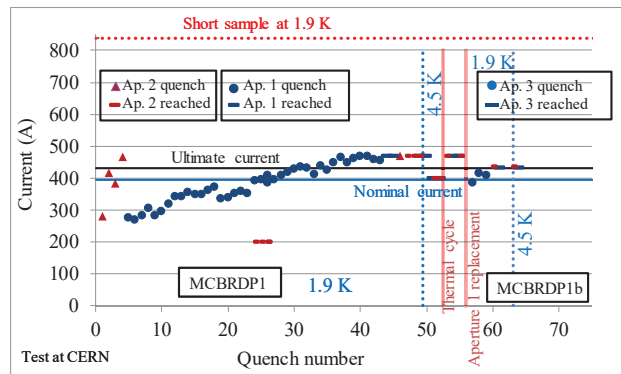
Fig. 7.5: Training performance of canted corrector first prototype.

Quench protection proved that quench back is the dominating mechanism. It can be initiated by a dump resistor of of 1.5 Ω; quench back increases the speed of discharge

(i.e. the increase of resistance of the coil) by a factor three (see Fig. 7.6).

Field quality was measured before assembly in the yoke and all harmonics were shown to be well within 3 units. After assembly a 10 units a_3/b_3 component was found to be due to the notches in the iron needed for coil alignment (see Fig. 7.3). As they were judged as non critical for beam dynamics, no design correction has been implemented.
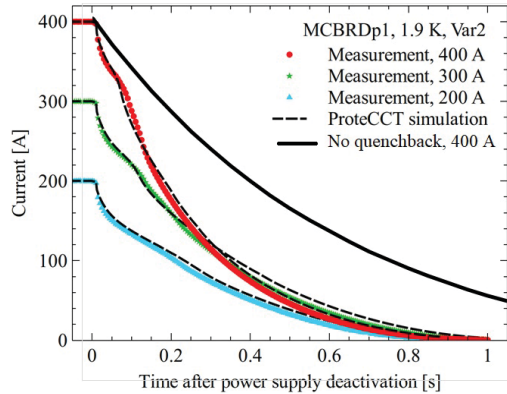
Fig. 7.6: Discharge during quench of the MCBRD corrector, measurements versus simulation, and case without considering quenchback.

7.4 Design changes

The only major design change was the decision of using a special tool to wind the 10 cables in the groove at the same time (see Fig. 7.7). This considerably simplified the coil winding, that can be performed as fast as one day per layer.

Fig. 7.87: Tooling allowing to wind ten strands in one go.

7.5 Setbacks and open issues

Even though this technology was a prima for CERN the development had no setbacks. The only open point is the slow training in virgin conditions of the first aperture of the

prototype, and the difference with respect to the second aperture.

7.6 Timeline

The main milestones of the canted dipole corrector development are the followings:

- August 2014: Beginning of the design study;
- August 2015: Selection of the canted cos theta design;
- March 2017: Beginning of collaboration and technology transfer to IHEP (Beijing);
- August 2017: Test of the first aperture of the short model;
- May 2018: Test of the second aperture of the short model at CERN;
- November 2018: Test of the prototype at CERN;
- May 2019: Beginning of prototype construction in WST (X'ian)
- January 2020: Test of the CERN prototype with one aperture replaced.

For this magnet the schedule constraint is given by the former manufacturing, that can take two weeks. Coil winding is quite fast, and can be done in one/two days. A production rate of one magnet every two months is assumed.

8. The superferric high order correctors

8.1 Accelerator requirements

The high order correctors are five types of magnets (quadrupole to dodecapole) needed to correct the tilt error of the triplet (skew quadrupole), and the high order field imperfections of the triplet and of the separation dipole (sextupole to dodecapole). The requirements in terms of integrated field (main field at 50 mm reference radius, integrated over the magnet length) are given in Table 8.1. They correspond to a maximum correction of an average tilt of the triplet of ±5 mrad, and of the following nonlinearities in the triplet: ±6.8 units of sextupole, ±5 units of octupole, ±2.6 units of decapole, ±6 units of normal dodecapole and ±1.5 units of skew dodecapole.

The magnets are used only at top energy, after the beam squeeze, and they are individually powered. Field quality requirements impose multipoles at reference radius below 100 units (ie below 1% of the main component). They have to be able to operate up to a 15 MGy radiation dose.

8.2 Design features

Since the very beginning of the project, a superferric technology based on coils wound with Nb-Ti wire around iron poles has been chosen (see Fig. 8.1 and 8.2). The design, carried out by INFN-Milano in LASA laboratory [58] relied

on the development and construction of a similar superferric sextupole developed in 2011-2012 for the FAIR and for the S-LHC study by CIEMAT [65,66].
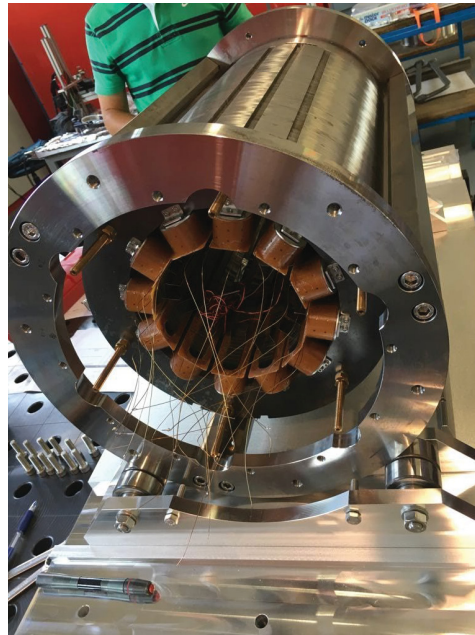
Fig. 8.1: Assembly of the dodecapole prototype coils in the iron laminations.

The main magnet parameters are listed in Table 8.1. As already discussed in Section 2.1, the magnet operate at 25-45% of the maximum current. The peak field on the coil is between 1.5 and 3.6 T; the coils are 150 mm long, with the exception of skew quadrupole and normal dodecapole whose length is about 500 mm. For all magnets except the quadrupole, an operational current not larger than 105 A is required to allowe reusing LHC power converter, giving a significant cost reduction. For the skew quadrupole a limit to 210 A is set. To match this requirement, a Nb-Ti strand diameter of 0.5 mm has been selected (0.7 mm for the skew quadrupole) and the coils are made with 200-750 turns. Insulation is made with S2-glass braid, and coils are impregnated with CTD-101K [58,61].

Coils are kept in position via metallic wedges that are pushed radially on the iron poles. These wedges also provide the necessary mechanical support to balance the electromagnetic forces.

Protection is done via energy extraction for the skew quadrupole, that has an inductance well larger than 1 H. For the other magnets quench propagation is enough to build up the required resistance to rapidly dump the current. A maximum hotpost temperature of 200 K is specified.

Sextupole, octupole and decapole full-size prototypes were

built in LASA laboratory; dodecapole and skew quadrupole prototypes were built in SAES-RIAL (Italy) since the size was not compatible with LASA infrastructure. For all magnets, desgin and follow up were provided by LASA laboratories.
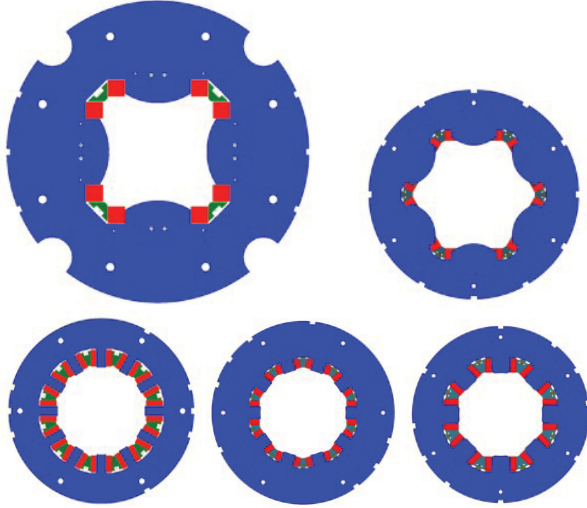
Fig. 8.2: Cross-sections of quadrupole, sextupole, octupole, decapole and dodecapole correctors.

Table. 8.1: Main requirements and parameters of the high order correctors.

Name	unit	MQXSF	MCSXF MCSSXF	MCOXF MCOSXF
Order	(adim)	2	3	4
Integrated strength	(T m)	0.700	0.095	0.069
Coil lenght	(mm)	457	192	172
Gradient	(T/m^{n-1})	34.8	224	3680
Coil peak field	(T)	3.6	2.23	2.09
Strand diameter	(mm)	0.7	0.5	0.5
N turn/pole	(adim)	754	288	372
Current	(A)	174	99	102
J overall	(A/mm²)	314	308	317
Loadline fraction	(adim)	0.44	0.31	0.31
Diff. inductance	(mH)	1530	213	220
Stored energy	(kJ)	30.8	1.72	1.55

Name	unit	MCDXF MCDSXF	MCTXF	MCTSXF
Order	(adim)	5	6	6
Integrated strength	(T m)	0.037	0.086	0.017
Coil lenght	(mm)	172	498	123
Gradient	(T/m^{n-1})	40480	585600	550400
Coil peak field	(T)	1.63	1.57	1.50
Strand diameter	(mm)	0.5	0.5	0.5

N turn/pole	(adim)	228	432	432
Current	(A)	92	85	84
J overall	(A/mm²)	286	264	261
Loadline fraction	(adim)	0.26	0.27	0.27
Diff. inductance	(mH)	120	805	177
Stored energy	(kJ)	0.668	3.63	0.732

8.3 Design validation via power tests

Power test at 4.2 K were systematically carried out at LASA laboratories on all prototypes. Verification at 1.9 K, together with field quality measurements were done at CERN. Results are shown in Figs. 8.3-8.7. The sextupole prototype reached operational current without training (see Fig. 8.3) and was powered up to 65% of short sample [59]. The octupole required few quenches to reach operational current (see Fig. 8.4) and was powered up to 63% of short sample [60]. Decapole and dodecapole reach operational current with one quench (see Fig. 8.5 and 8.6) [62,63]. In all cases no retraining was observed after thermal cycle. The skew quadrupole had a somewhat different phenomenology (see Fig. 8.7), with a 10 quenches to reach nominal current and another 10 to rach ultimate current. Note that in the quadrupole not only the forces are larger, but also that the loadline fraction is 44% compared to 26-31% as in the higher order magnets. Field quality was measured in sextupole, octupole and decapole, with results well 10 units, i.e. 10 times smaller than the accetance tolerances. Saturation was measured to be in agreement with the magnetic 3D model [64].
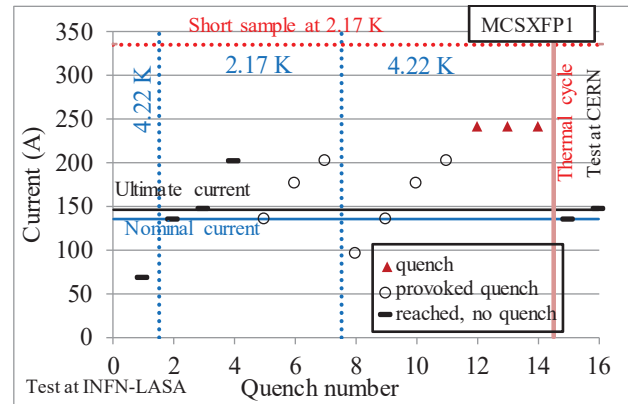
Fig. 8.3: Training of sextupole corrector prototype.
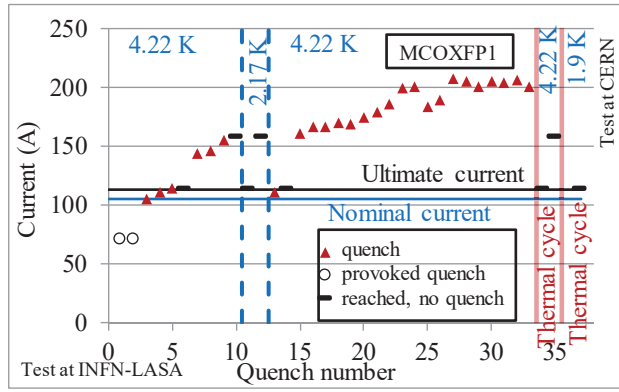
Fig. 8.4: Training of octupole corrector prototype.

Fig. 8.5: Training of decapole corrector prototype.
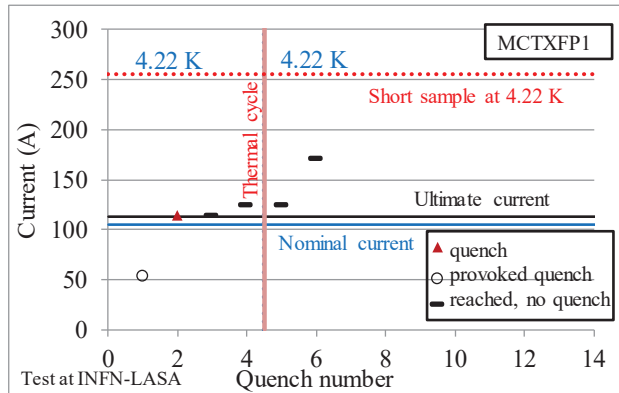
Fig. 8.6: Training of dodecapole corrector prototype.

Fig. 8.7: Training of quadrupole corrector prototype.

8.4 Design changes

A first change was introduced at the beginning of the project, namely to fit the 120 A limit for the ultimate current in order to reuse the LHC power converter. This first prototype sextupole did not include this constraint, and had a slightly larger current [58]. In the iteration of the design, additional turns were added to fit the current constraint.

The second change concerned an iteration on the material for the coil box; three different materials were tested in the initial phase, namely 3D printed ULTEM, Duratron, and BT resin S2 reinforced. After several test, the latter was selected [61].

A third change was the 50% increase of the field integral requirements for sextupole octupole and decapole to cope with larger unallowed low order multipoles in the triplet (see Section 3). The field integral increase was obtained via a ~30% longer magnetic length. Space was recovered by reducing the length of the skew quadrupole, that revealed to be overdimensioned with respect to alignement tolerances.

8.5 Setbacks and open issues

The first power test of the quadrupole corrector was interrupted after the 15th quench due to the appearance of an electrical interturn short. The origin of the problem was traced back to a weakness in the insulation of the coil at the location of the wire exit. After this finding, the design of the insulation at the coil lead and the design of all connection plates has been reinforced in all magnets, even though the previous produced coils did not show weakness. The test of the second assembly was succesful (see Fig. 8.7).

A source of concern is the long training seen in the skew quadrupole, and the limited memory after thermal cycle, where two quenches were needed to reach nominal current. An iteration is being done on the design of the skew quadrupole coil supports to improve this aspect.

8.6 The round coil superferric corrector

In the initial phase of the design, the option of a superferric magnet based on MgB_2 conductor was also considered. The major showstopper for using this technology in the superferric option was found to be the minimum curvature radius of the MgB_2 tape, that had to be larger than 100 mm. To avoid the small curvature radii, an alternative design based on a concept developed in the 70's [91] and further investigated in the 10's [92] has been explored [93]. The idea is to have a round coil whose solenoidal field is shaped in a multipolar transverse field thanks to the iron shape (see Fig. 8.8).

This design had the main advantage of having not only much larger curvature radii for the coil, but also to use the same coil for producing different multipolar fields via the assembly in a different iron yoke. The drawback of this design is that compared to a standard superferric magnet one loses about a factor two in the integrated gradient. In the case of HL-LHC interaction region, using this design would have required doubling the space for the corrector package, i.e. 3-4 additional meters. Unfortunately this space was not available in the lay-out, and the option has been abandoned.
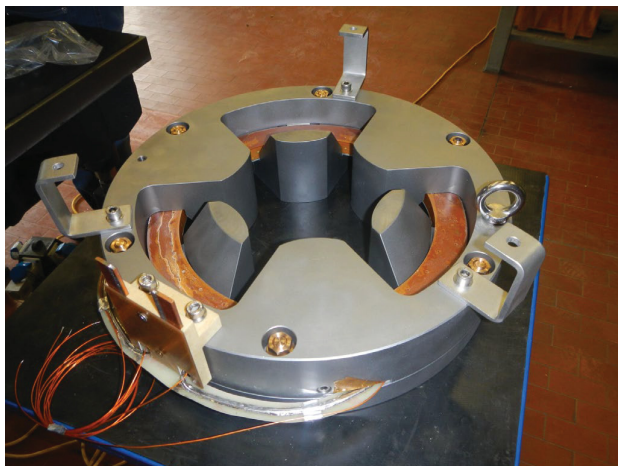
Fig. 8.8: The final assembly of the sextupole corrector based on round coil superferric design and MgB_2 conductor.

INFN pursed the construction of a sextupole demonstrator, i.e. half of a prototype, based on a MgB_2 wire, able to carry 382 A/mm^2 overall current density at 2.12 T and 4.2 K. In the RCSM configuration, nominal field is reached with a 150 A current, and the magnet operates at 45% of the loadline. The magnet test was carried out in LASA [94], and the magnet reached nominal current without quench, and was limited at 82% of the short sample field (see Fig. 8.8)
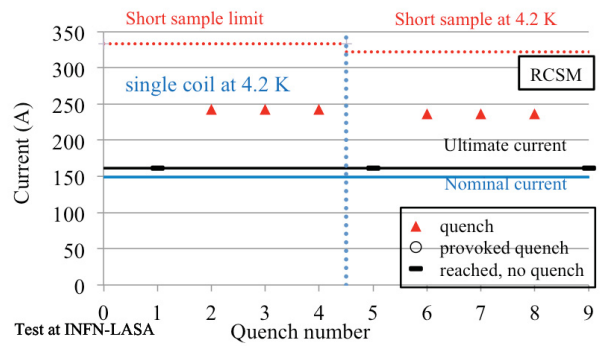
Fig. 8.8: Training performance of sextupole corrector based on RCSM design and MgB_2 conductor.

8.7 Timeline

The main milestones of the high order correctors development are the followings:

- <u>March 2014</u>: Signature of the collaboration agreement between CERN and INFN-LASA to develop design, manufacture and test five types of high order correctors;
- <u>February 2016</u>: test of the prototype sextupole;
- <u>March 2017</u>: test of the prototype octupole;
- <u>August 2017</u>: Signature of the collaboration agreement between CERN and INFN-LASA to manufacture the high order corrector series;
- <u>September 2017</u>: test of the prototype decapole;
- <u>September 2017</u>: Signature of contract with SAES-RIAL for manufacturing of dodecapole and quadrupole prototypes.
- <u>April 2018</u>: change of corrector strenght for quadrupole, sextupole, and octupole;
- <u>October 2018</u>: test of prototype dodecapole;
- <u>February 2019</u>: test of prototoype quadrupole, interrupted by an electrical short;
- <u>July 2019</u>: Second test of the prototype quadrupole, after replacement of two coils.

Main bottleneck for the schedule is the coil winding and impregnation. This is particularly critical for magnets with higher number of poles. A production rate of one magnet every two to three weeks is assumed.

Conclusions

This paper describes the superconducting magnets needed for the HL-LHC interaction regions, that are now in transition between the model/prototype phase and the series production. It is a short series of about 100 magnets of 6 different types: one quadrupole based on Nb_3Sn technology, two main dipoles and three correctors based on Nb-Ti technology.

The triplet represents a significant advancement in the accelerator magnets, with peak field 50% larger than the Nb-Ti LHC dipoles (12 T versus 8 T) and twice accumulated midplane transverse stress in operational conditions (120 MPa versus 60 MPa).

The HL-LHC main dipoles are in line with the existing Nb-Ti technology, but present particular challenges:

- D1 is a 5.6 T magnet presenting a very large (100 MPa) accumulation of prestress in the midplane due to its large aperture;
- D2 is a double aperture magnet were the coils are slightly asymmetric to compensate for the magnetic cross-talk, to reach the string target on field quality;
- The three correctors rely on three different designs, namely a nested horizontal vertical dipole based on double collaring, a canted cos theta dipole and several superferric high order correctors.

The main features of the magnets have been discussed in section 2 and 3, presenting the reasons for the selection of the main parameters and the main challenges. In the following sections, we presented for each magnet the requirements, the design selection, and the results of the short models and prototypes validating the design. A special section is devoted to open issues and setbacks/failures, plus a timeline of the development.

The triplet program was validated through the test of five short models and three prototypes, with a joint effort between CERN and a consortium of US laboratories (FNAL, BNL and LBNL). The magnets proved to be able to reach nominal current in four short models and two prototypes. Two production lines for short coils, and two production lines for 4.2-m-long coil have been validated, showing to be able to manufacture coils reaching the required performance. The program had two understood failure cases, and two cases of missing or partially achived performance, most probably related to conductor degradation, whose origin has not been yet clearly understood. Performance reproducibility is the main issue on the table at the moment of writing. However, the MQXF program proved a large potential of Nb$_3$Sn technology, in particular:

- Short models proved the existence of a wide range of assembly parameters (in terms of coil precomporession) that provide the required performance;
- All magnets reaching nominal current at 1.9 K showed ability of reaching nominal current (and more) at 4.5 K, thus proving a large temperature margin;
- All magnets showed no need of retraining to operate at nominal current after thermal cycle; in many cases no retraining was needed to operate at ultimate current.

Finally, the MQXF magnet protection relies on CLIQ, i.e. a novel quench protection method based on heating the magnet via eddy currents generated by a capacitor discharge.This method has been sucesfully tested on the short models.

The separation dipole D1 design has been validated through the construction of three short models. Design and construction was done in KEK, Japan. Iterations have been required to optimize the precompression and field quality. At the end, all three models reached the target performance, the only missing point is the field quality fine tuning to minimize the sextupolar component.

The recombination dipole D2 design has been validated on one aperture, the test of the repaired second aperture being foreseen for spring 2020. Design was done in INFN-Ge, Italy, and construction ins ASG Superconductors. The strategy for the field quality cross-talk compensation based on an asymmetric coil geometry has been validated succesfully at room temperature. The design required an iteration on the transition from the coil to the cable lead coming out from the winding pole. The initial design weakness provoked two shorts and one severely damaged cable.

The nested corrector proved the soundness of a double collared structure, a prima in magnet technology. Design and manufacturing was done in CIEMAT, Spain, with collaring at CERN. The double collaring allows to withstand the large torque when both magnets are powered. The prototype reached most of the required performance after few iterations on the azimuthal precompression of the straght part and of the heads. It has been validated on one prototype, and a second model will be tested in spring 2020.

The D2 corrector using the canted cos theta layout proved the flexibility and the advantages of this design requiring very little tooling, and simple and fast assembly. The magnet development, first of this design to be developed at CERN, was succesful and now the technology is being transfered to China collaboration led by IHEP.

The superferric correctors proved to be a robust technology, and the design and prototype construction was done in INFN-LASA, Italy, with the longer magnets manufactured in SAES-RIAL. Validation has been completed with succesful tests, with few iterations on the design to improve the electrical insulation and the coil support.

The project now enters the construction phase, the main challenge being the scaling from short model to prototypes for the main magnets. A difficult feature of the project is the small number of magnets to be built, allowing very limited feedback during production.

For the Nb$_3$Sn case, that is the most innovative technology for superconducting magnets in accelerators, the HL-.LHC project will provide a statistics on the performance of 30

magnets and 5 prototypes built with identical cross-section and two different lengths, with three production lines. This will allow drawing precious conclusions for the potential of the Nb$_3$Sn technology required in a high field collider to be built after the HL-LHC era.

References

[1] Bruning O, et al., Eds. 2004 CERN-2004-003 (LHC design report)

[2] Perin R, 1989 *IEEE Transaction on Magnetics* **25** 1632-5 (first reference about LHC dipoles)

[3] Rossi L, 2003 *IEEE Transaction on Applied Superconductivity* **13** 1221-28 (LHC dipole production)

[4] A.A V.V. 1984 CERN 84-10 (first proposal of LHC)

[5] The LHC study group, 1995 CERN/AC/95-05 (prototypes)

[6] Wyss C, 1999 *Particle Accelerator Conference* 149-153 (towards series)

[7] Billan J, et al.1999 *IEEE Transaction on Applied Superconductivity* **9** 1039-44 (End of prototype phase)

[8] Lamont M, et al. 2009 *Particle Accelerator Conference* 1412-4 (LHC commissioning)

[9] ATLAS collaboration 2012 *Phys Lett B* **716** 1-29

[10] CMS collaboration 2012 *Phys Lett B* **716** 30-61

[11] Rossi L, 2012 *Journal of Cryogenics and Superconductivity Society Japan* **47** (start of HL LHC)

[12] Strait J, et al. 2003 *Particle Accelerator Conference* 42-44 (First trace of LHC upgrade)

[13] Bruning O, et al. 2002 LHC Project Report 626 (The thick report on LHC upgrade)

[14] Koutchouk J P, 2006 *European Particle Accelerator Conference* 556 (Koutchouck contribution to LHC upgrade)

[15] Bruning O, Rossi L, Eds. 2015 *Advanced series on Directions in High Energy Physics* **24** World Scientific (hilumi book)

[16] Apollinari G, et al., Eds. 2017 CERN-2017-007-M (HL LHC design report)

[17] Todesco E, et al. 2014 *IEEE Transaction on Applied Superconductivity* **24** 4003305 (HL-LHC aperture selection)

[18] Ajima, et al. 2005 *Nucl. Instrum. Meth. A* **550** 499-513 (MQXFA)

[19] Bossert R, et al. 2004 *IEEE Transaction on Applied Superconductivity* **14** 187- 190 (MQXFB)

[20] Feher S, et al. 2006 *IEEE Transaction on Applied Superconductivity* **16** 437-440 (MQXFA/B)

[21] Ferracin P, et al.2005 *IEEE Transaction on Applied Superconductivity* **15** 1132-35 (LARP)

[22] Gourlay S, et al. 2006 *IEEE Transaction on Applied Superconductivity* **16** 324-327 (LARP)

[23] Wanderer P 2009 *IEEE Transaction on Applied Superconductivity* **19** 1208-11 (LARP)

[24] Caspi S 2010 *IEEE Transaction on Applied Superconductivity* **20** 144-7 (HQ)

[25] Ambrosio G, et al. 2008 *IEEE Transaction on Applied Superconductivity* **13** 268-72 (LQ)

[26] Ambrosio G, et al. 2013 *IEEE Transaction on Applied Superconductivity* **23** 4002204 (LQ)

[27] Ferracin P, Ambrosio G, et al, 2016 *IEEE Transaction on Applied Superconductivity* **26** 4000207 (MQXF design)

[28] Ferracin P, Ambrosio G, et al, 2019 *IEEE Transaction on Applied Superconductivity* **29** 4000207 (MQXF test results)

[29] Todesco E 2018 *IEEE Transaction on Applied Superconductivity* **28** 4008809 (MQXF and 11 T)

[30] Scanlan R, Dietderich D R 2003 *IEEE Transaction on Applied Superconductivity* **13** 1536-1541 (CDP US)

[31] Weijers H W, ten Kate H, van Oort J M, 1993 *IEEE Transaction on Applied Superconductivity* **3** 1334 (degradation Nb3Sn)

[32] ten Haken B, et al., 1999 *Journal of Applied Physics* **85** (degradation Nb3Sn)

[33] Savary F 2017 *IEEE Transaction on Applied Superconductivity* **27** 4003505 (11 T)

[34] Tommasini D, et al. 2017 *IEEE Transaction on Applied Superconductivity* **27** 4000405 (FCC)

[35] Tommasini D, et al. 2018 *IEEE Transaction on Applied Superconductivity* **28** 4001305 (FCC)

[36] Xu Q, et al. 2012 *IEEE Transaction on Applied Superconductivity* **22** 4901404 (first design)

[37] Nakamoto T, et al. 2015 *IEEE Transaction on Applied Superconductivity* **25** 4000505 (D1 construction, final design)

[38] Sugano M, et al. 2017 *IEEE Transaction on Applied Superconductivity* **27** 4002409 (D1 test S1)

[39] Sugano M, et al. 2018 *IEEE Transaction on Applied Superconductivity* **28** 4000805 (D1 training 1b)

[40] Enomoto S, et al. 2018 *IEEE Transaction on Applied Superconductivity* **28** 4004505 (D1 magn measurements)

[41] Nilsson E, et al. 2018 *IEEE Transaction on Applied Superconductivity* **28** 4003005 (D1 ends field model)

[42] Suzuki K, et al. 2019 *IEEE Transaction on Applied Superconductivity* **29** 4000905 (D1 Test S2)

[43] Sugano M, et al. 2019 *IEEE Transaction on Applied Superconductivity* **29** 4003607 changes in design from 1 to 2)

[44] Farinon S, et al. 2016 *IEEE Transaction on Applied Superconductivity* **26** 4001504 (D2 design)

[45] Fabbricatore P, et al. 2018 *IEEE Transaction on Applied Superconductivity* **28** 4000105 (D2 short model)

[46] Bersani A, et al. 2019 *IEEE Transaction on Applied Superconductivity* **29** 4003305 (D2 from model to proto)

[47] Kashikin V, Zlobin A 2007 *Particle Accelerator Conference* **464-466** (D2 proposal with asymmetric coil)

[48] Ogitsu T, et al. 2005 *IEEE Transaction on Applied Superconductivity* **15** 1175-80 (JPARC combined f magnets)

[49] Garcia-Matos J, et al. 2016 *IEEE Transaction on Applied Superconductivity* **26** 4102005 (MCBXF design)

[50] Garcia-Matos J, et al. 2018 *IEEE Transaction on Applied Superconductivity* **28** 4101005 (MCBXF design)

[51] Garcia-Matos J, et al. 2019 *IEEE Transaction on Applied Superconductivity* **29** 4002205 (MCBXF design / construction)

[52] Kirby G, et al. 2017 *IEEE Transaction on Applied Superconductivity* **27** 4002805 (CCT design)

[53] Kirby G, et al. 2018 *IEEE Transaction on Applied Superconductivity* **28** 4002205 design (CCT design)

[54] Mangiarotti F, et al. 2019 *IEEE Transaction on Applied Superconductivity* **29** 4002305 design (CCT test)

[55] Meyer D I and Flasck R 1970 *Nuclear Instruments and Methods* **80** 339-341. (first CCT)

[56] Goodzeit C. L., et al 2003 *IEEE Transaction on Applied Superconductivity* **13** 1365-8 (Meinke contribution)

[57]   Caspi S, et al 2014 *IEEE Transaction on Applied Superconductivity* **24** 4001804 (CCT for high field)

[58]   Volpini G, et al. 2015 *IEEE Transaction on Applied Superconductivity* **25** 4002605 (superferric design)

[59]   Statera M, et al. 2017 *IEEE Transaction on Applied Superconductivity* **27** 4003205 (sextupole test)

[60]   Statera M, et al. 2018 *IEEE Transaction on Applied Superconductivity* **28** 4008705 (octupole)

[61]   Sorbi M, et al. 2018 *IEEE Transaction on Applied Superconductivity* **28** 4100205 (design final and status)

[62]   Statera M, et al. 2019 *IEEE Transaction on Applied Superconductivity* **29** 4004305 (decapole)

[63]   Sorbi M, et al. 2019 *IEEE Transaction on Applied Superconductivity* **29** 4001905 (dodecapole)

[64]   Fiscarelli L, et al. 2019 *IEEE Transaction on Applied Superconductivity* **29** 4003505 (magnetic measur HO correc)

[65]   Abramian P, et al. 2012 *IEEE Transaction on Applied Superconductivity* **22** 4902104 (superferric FAIR quad)

[66]   Abramian P, et al. 2013 *IEEE Transaction on Applied Superconductivity* **23** 4101204 (superferric SLHC)

[67]   Tollestrup A, Todesco E, 2008 *Rev. Sci. Accel. Tech.* 1 185-210 (Review about accelerator magnets)

[68]   Ravaioli E, Kirby G et al 2015 *IEEE Transaction on Applied Superconductivity* **22** 4001305 (CLIQ)

[69]   A. Verweij, et al. 2016 *IEEE Transaction on Applied Superconductivity* **26** 4000705 (training LHC dipole)

[70]   E. Todesco, et al. 2017 *IEEE Transaction on Applied Superconductivity* **27** 4702807 (training LHC dipole)

[71]   Rossi L, Todesco E 2007 *Phys. Rev. STAB* **10** 112401 (scaling law dipoles)

[72]   Rossi L, Todesco E 2006 *Phys. Rev. STAB* **9** 102401 (scaling law quadrupoles)

[73]   Fessia P, Regis F and Todesco E, 2009 *IEEE Transaction on Applied Superconductivity* **19** 1203-1207 (scaling forces dip)

[74]   Fessia P, Regis F and Todesco E, 2007 *IEEE Transaction on Applied Superconductivity* **17** 1269-72 (scaling forces qua)

[75]   Todesco E 2013 CERN 2013-006 10-16 (scaling prote)

[76]   Cooley L, et al. 2017 *IEEE Transaction on Applied Superconductivity* **27** 6000505 (Strand specs etc US)

[77]   Bordini B, et al. 2017 *IEEE Transaction on Applied Superconductivity* **27** 6000706 (PIT)

[78]   Izquiredo Bermudez S, et al. 2018 *IEEE Transaction on Applied Superconductivity* **28** 4008406 (Sprotection heaters)

[79]   Levitan J, et al. 2019 *IEEE Transaction on Applied Superconductivity* **29** 6000904 (Strand production US)

[80]   Pong I, et al. 2019 *IEEE Transaction on Applied Superconductivity* **29** 6001505 (Cable production US)

[81]   Chlachidze G, et al. 2017 *IEEE Transaction on Applied Superconductivity* **27** 4000205 (Test MQXFS1)

[82]   Stoynev S, et al. 2018 *IEEE Transaction on Applied Superconductivity* **28** 4001705 (Test MQXFS1a b c d)

[83]   Bajas H, et al 2018 *IEEE Transaction on Applied Superconductivity* **28** 4007006 (MQXFS3 and MQXFS5)

[84]   Mangiarotti F, et al. 2019 *IEEE Transaction on Applied Superconductivity* **29** 4001705 (MQXFS3 and MQXFS4)

[85]   Izquierdo Bermudez S, et al. 2019 *IEEE Transaction on Applied Superconductivity* **29** 4901705 (FQ in MQX)

[86]   Protection short

[87]   Ravaioli E, et al. 2019 *IEEE Transaction on Applied Superconductivity* **29** 4701405 (CLIQ in MQXFAP1)

[88]   Fleiter J, et al. 2017 *IEEE Transaction on Applied Superconductivity* **27** 4004305 (Change of cable)

[89]   Anarella M, et al. 2003 *Nuclear Instruments and methods* **A 499** 280-315 (RHIC dipoles)

[90]   Sorbi M, et al. 2008 *IEEE Transaction on Applied Superconductivity* **18** 138-141 (SIS300 design)

[91]   Malyshev I F, U. S. Patent 1698 890/26-25, Oct. 12 1973 (RCSM patent)

[92]   Kashikhin V 2010 *IEEE Transaction on Applied Superconductivity* **20** 196-200 (RCSM magnet design)

[93]   Mariotto S, et al. 2018 *IEEE Transaction on Applied Superconductivity* **28** 4003305 (RCSM design)

[94]   Mariotto S, et al. 2019 *IEEE Transaction on Applied Superconductivity* **29** 4004505 (RCSM single coil test)

Appendix A: stress estimate in cos theta magnets

In this section we give a more refined estimate for the accumulation of the stress in the midplane in a cos-theta dipole and quadrupole. Following the approach outlined in [], Eq. (3) for a dipole one can estimate the accumulation of stress in the midplane at the position

$$\sigma(x) = \frac{j^2\mu_0\sqrt{3}}{6\pi(r+x)}[2(r+x)^3 + r^3 - 3(r+x)^2(r+w)]$$
(A.1)

where x spans from 0 (at the magnet bore) to the coil width w (on the outer ardius of the coil). Since one has that for a 60° coil one has

$$B = \gamma j w = \frac{\mu_0\sqrt{3}}{\pi}jw \qquad (A.2)$$

the previous equation can be cast in the form

$$\sigma(x) = \frac{Bjr}{2}\frac{2(r+x)^3+r^3-3(r+x)^2(r+w)}{3wr(r+x)} \qquad (A.3)$$

and for $x=0$, i.e. on the edge of the aperture, one finds

$$\sigma_r = \sigma(0) = \frac{Bjr}{2}\frac{1}{3wr^2}[-3wr^2] = -\frac{Bjr}{2} \quad (A.4)$$

Therefore the maximum of the stress is given by

$$\sigma_{max} = \sigma_r \text{Max}_{0<x<w}\frac{2(r+x)^3+r^3-3(r+x)^2(r+w)}{3wr(r+x)} \qquad (A.5)$$

For a quadrupole one can compute (see Eq. (1) in [], assuming a 30° sector coil)

$$\sigma(x) = \frac{j^2\mu_0\sqrt{3}}{16\pi}\frac{(r+x)^4 - r^4 + 4(r+x)^4 ln\left(\frac{r+w}{r+x}\right)}{(r+x)^2}$$
(A.6)

where x spans from 0 to the coil width w. Since one has that for a 30 degrees coil one has

$$G = \gamma j \ln\left(1 + \frac{w}{r}\right) = \frac{\mu_0\sqrt{3}}{\pi} j \ln\left(1 + \frac{w}{r}\right) \qquad (A.7)$$

the previous equation can be cast in the form

$$\sigma(x) = \frac{jG}{16} \frac{(r+x)^4 - r^4 + 4(r+x)^4 \ln\left(\frac{r+w}{r+x}\right)}{(r+x)^2 \ln\left(1 + \frac{w}{r}\right)} \qquad (A.8)$$

and for $x=0$, i.e. on the edge of the aperture, one finds

$$\sigma_r = \sigma(0) = \frac{jG}{4} r^2 \qquad (A.9)$$

Therefore the maximum of the stress is given by

$$\sigma_{max} = \sigma_r Max_{0<x<w} \frac{(r+x)^4 - r^4 + 4(r+x)^4 \ln\left(\frac{r+w}{r+x}\right)}{4r^2(r+x)^2 \ln\left(1 + \frac{w}{r}\right)} \qquad (A.10)$$

In Table VI we give the stress at the bore and the peak stress in the mdiplane for the HL-LHC cos theta magnets, for the 11 T and for the LHC dipole

	r	w	σ_r	σ_{max}	σ_{max} / σ_r
	(mm)	(mm)	(MPa)	(MPa)	(adim)
11 T	30	28	90	116	1.28
MQXF	75	36	87	110	1.26
LHC MB	30	31	41	55	1.32
MBXF	75	15.4	94	99	1.05
MBRD	52.5	15.4	56	61	1.08
MCBXF	75	9	25	25	1.03